**Distribution Agreement**

In presenting this thesis as a partial fulfillment of the requirements for a degree from Emory University, I hereby grant to Emory University and its agents the non-exclusive license to archive, make accessible, and display my thesis in whole or in part in all forms of media, now or hereafter now, including display on the World Wide Web. I understand that I may select some access restrictions as part of the online submission of this thesis. I retain all ownership rights to the copyright of the thesis. I also retain the right to use in future works (such as articles or books) all or part of this thesis.

Masin Kearney March 17, 2025

# A phosphopeptide enrichment strategy for investigating phosphorylation in Alzheimer's disease and related tauopathies

By

Masin Kearney

Nicholas Seyfried
Adviser

Department of Biology

Nicholas Seyfried
Adviser

Leah Roesch
Committee Member

Astrid Prinz
Committee Member

2025

# A phosphopeptide enrichment strategy for investigating phosphorylation in Alzheimer's disease and related tauopathies

By

Masin Kearney

Nicholas Seyfried
Adviser

An abstract of
a thesis submitted to the Faculty of Emory College of Arts and Sciences
of Emory University in partial fulfillment
of the requirements of the degree of
Bachelor of Science with Honors

Department of Biology

2025

Abstract

A phosphopeptide enrichment strategy for investigating phosphorylation in Alzheimer's disease and related tauopathies

By Masin Kearney

Alzheimer's disease (AD) is a tauopathy characterized by cognitive decline and neuropathological changes driven by the aggregation of extracellular amyloid-beta plaques and intracellular tau-containing neurofibrillary tangles (NFTs). Tau is hyperphosphorylated prior to NFT formation, suggesting that abnormal phosphorylation contributes to neurotoxicity by altering protein structure and function. In addition to tau hyperphosphorylation, global phosphorylation-dependent signaling cascades are implicated in the pathogenesis of tauopathies. Other tauopathies that share tau pathology with AD include frontotemporal dementia with parkinsonism (FTDP) and progressive supranuclear palsy (PSP). However, overlapping clinical and neuropathological features among these diseases complicate differential diagnosis, and the absence of effective treatments underscores the need for therapeutic development. Phosphoproteomics enables the enrichment and identification of proteins within these signaling pathways, providing insight into potential biomarkers and therapeutic targets. However, studying phosphoproteins is challenging due to their low abundance and the presence of non-phosphorylated isoforms. To address this, immobilized metal affinity chromatography (IMAC) followed by label-free liquid chromatography-tandem mass spectrometry (LC-MS/MS) was used to investigate the phosphoproteome. Brain lysates from AD, FTDP, PSP, and non-demented control frontal cortex brain tissue samples were digested and subjected to phosphopeptide enrichment using Fe-NTA magnetic beads, followed by data-dependent acquisition LC-MS/MS analysis. Raw MS data were processed with FragPipe, missing values were imputed, and statistical tests were performed to identify differentially enriched proteins and gene ontology categories. Consistent with previous studies, microtubule-associated protein tau (MAPT) was more highly phosphorylated in AD brain tissue than in FTDP, PSP, or control samples. Future work will scale and automate phosphopeptide enrichment from brain tissue and additional biofluids, such as cerebrospinal fluid (CSF) and plasma, to further explore AD biomarkers and underlying mechanisms. A more comprehensive understanding of biomarkers across brain, CSF, and plasma may enable non-invasive diagnostics and uncover novel therapeutic avenues for tauopathies.

# A phosphopeptide enrichment strategy for investigating phosphorylation in Alzheimer's disease and related tauopathies

By

Masin Kearney

Nicholas Seyfried
Adviser

An abstract of
a thesis submitted to the Faculty of Emory College of Arts and Sciences
of Emory University in partial fulfillment
of the requirements of the degree of
Bachelor of Science with Honors

Department of Biology

2025

Acknowledgements

I would like to sincerely thank Dr. Nicholas Seyfried for welcoming me into his laboratory and for providing the mentorship, guidance, and resources necessary to complete this project. I am deeply grateful for the trust and confidence you had in my abilities, which prepared me to become a truly independent researcher.

I am especially grateful to Sarah Shapley for her invaluable support throughout this work and for generously sharing her homogenized brain tissue samples. This project would have crashed and burned dozens of times without her instantaneous Teams responses to all of my questions—even when she was on Do Not Disturb. She loved to joke about not knowing what she was doing, but I am incredibly thankful for her expertise and guidance. More than that, she showed me what it truly means to be a scientist, inspiring me to pursue this career path.

I also extend my gratitude to Dr. Caroline Watson for her expertise in mass spectrometry and for helping me design a feasible and impactful project. She was always there for a reality check when I got overwhelmed and had the magical ability to weave a beautiful narrative from my data even when I hit some experimental roadblocks. We constantly were teaching each other new things, and our chats in the office were some of the highlights of my time in lab.

Additionally, I would like to thank Dr. Joshna Gadhavi for her assistance with lab materials. Thank you, Dr. Eddie Fox, for always being there to plan, organize, coordinate, and manage anything and everything. I am also appreciative of Dr. Adam Trautwig, Dr. Eric Dammer, and the rest of the Seyfried lab for their insights and support with our bioinformatics pipelines. Additionally, thank you to everyone in the Seyfried lab for attending my presentations and always providing the feedback and encouragement that pushed me to be a better scientist. It has been a privilege to spend the past four years working alongside you all, and you have forever shaped my perspective on what it means to do science.

A heartfelt thank you to my parents for listening patiently as I explained tau phosphorylation to you again and again. Thank you for answering my emotional phone calls as I walked home from lab, stressed about finishing my thesis on time. Most of all, thank you for trying your best to learn all you could about Alzheimer's disease and for giving me the support and resources that allowed me to devote these past four years to research.

Last but certainly not least, thank you to my incredible friends—Grace, Trinity, and Alyssa. I truly could not have finished this project without you. From early mornings in coffee shops to late nights in the library, you were always there when I needed you. We laughed, brainstormed, ate way too much pizza and ice cream, and laughed some more. Your unwavering support, encouragement, and patience (even through my endless rants about phosphopeptides) meant the world to me. Thank you for reminding me to take breaks and to keep sight of the bigger picture. I am so grateful to have had your love and support through it all.

Table of Contents

Tables & Figures

## Chapter 1: Introduction

### 1.1 Phosphorylation

Phosphorylation is a post-translational modification (PTM) that changes the electrostatic character of a protein through the covalent addition of a negatively-charged hydrophilic phosphate group ($PO_4^{3-}$) to the polar R group of an amino acid (Figure 1).[1] Canonical phosphorylation occurs on the hydroxyl of a serine, threonine, and tyrosine (STY) residues, initiating changes to protein structure and function. Due to its fast kinetics and reversibility, this modification serves as a dynamic regulator in biological systems.[2]

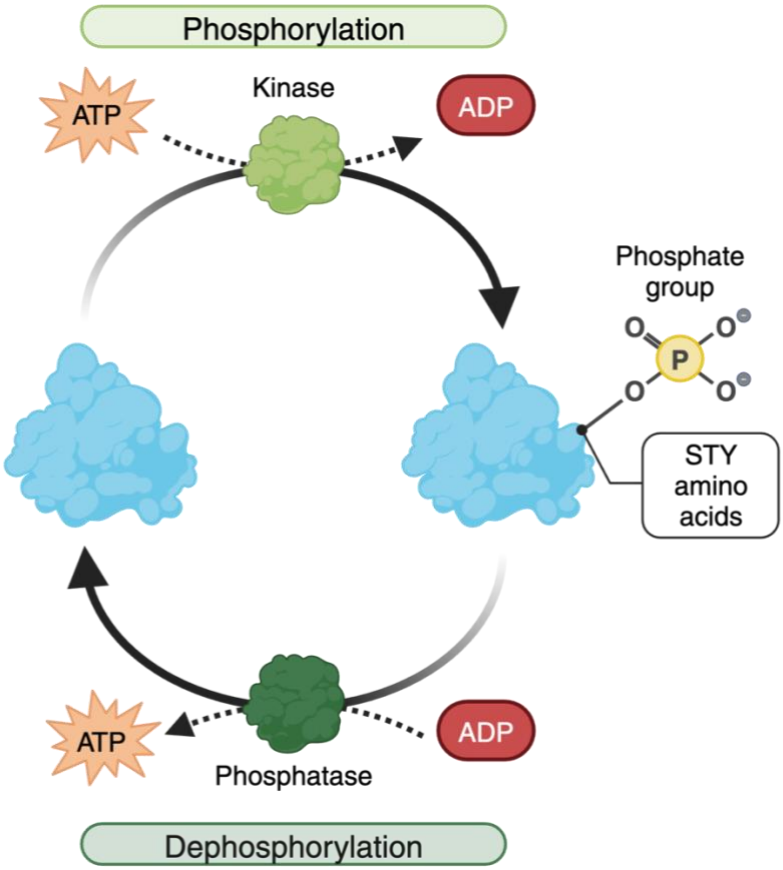


**Figure 1.** Phosphorylation and dephosphorylation of proteins by kinases and phosphatases.

Adenosine triphosphate (ATP) is an abundant phosphate donor, contributing to the ubiquitous role of phosphorylation within the body.[3] Beyond regulating ATP production and recycling, phosphorylation governs signal transduction by mediating transient protein-protein interactions, driving subcellular or membrane translocation, influencing secondary PTM addition or removal, modulating protein order and disorder, and inducing dimerization.[4,5] Phosphorylation at an enzyme's binding site can alter its binding energy, with multi-site phosphorylation influencing binding selectivity at the residue level.[2] Additionally, it may induce a conformational change that induces allosteric activation or blocks access to the active site to inhibit activation.

The addition of phosphate groups regulates diverse processes such as metabolic pathways, membrane transport, and gene transcription. Studies have shown that in humans proteins have an average of two phosphorylated sites, but heterooligomers involved with catalytic, hydrolase, transferase, or signal transducer activities are more likely to have more phosphorylated sites than other proteins.[2] Protein kinases belong to these phospho-signaling cascades, where they catalyze phosphorylation in response to external and internal stimuli.[4] Such processes are further regulated by the activation of phosphatases, which dephosphorylate proteins in response to different stimuli to provide dual regulation of phosphorylation-dependent signaling. The human genome includes approximately 500 protein kinases and 200 protein phosphatases.[6,7] Kinases share a structurally conserved catalytic domain, but phosphatase structure is less understood.[8]

### 1.2 Phosphorylation in Disease

*Cancer*

Dysregulation of kinase and phosphatase activity occurs under pathological conditions, with mutations affecting phosphorylation being prevalent in cancer signaling pathways. Studies show that cancer-associated kinases are twice as likely to both gain or lose phosphorylation sites compared to control kinases.[9] For example, phosphorylation dysregulation is relevant in prostate cancer, where elevated levels of phosphorylated Protein Kinase B (Akt), a key component of the

Phosphatidylinositol 3-kinase (PI3K) signaling pathway, are associated with an increased risk of prostate-specific antigen (PSA) failure and poor clinical outcomes.[10] In breast cancer cells, both serine and tyrosine phosphorylation have been shown to activate signal transducers and activators of transcription (STAT) proteins under hypoxic conditions, indicating the role phosphorylation may play in breast tumorigenesis via the Janus kinase (JAK)-STAT pathway.[11] Furthermore, the tumor suppressing activity of Protein phosphatase 2A (PP2A) is reduced in many pancreatic cancer cell lines due to the overexpression of endogenous PP2A inhibitors, such as cancerous inhibitor of PP2A (CIP2A) and SET nuclear proto-oncogene (SET).[12]

*Neurodegeneration*

Phosphorylation is also implicated in protein aggregation and neurotoxicity in neurodegenerative diseases.[13] Phosphorylated $\alpha$-synuclein accumulates in insoluble aggregates called Lewy Bodies, characteristic of Lewy Body Disorders such as Parkinson's disease (PD), Parkinson's disease with dementia (PDD), and dementia with Lewy Bodies (DLB).[14,15] Hyperphosphorylated tau, which forms the neurofibrillary tangles associated with Alzheimer's disease (AD), often presents as a co-pathology in many cases of Lewy body disorders.[16]

### 1.3 Tauopathies

*Tau*

Tau, a microtubule-associated protein, is an intrinsically disordered protein (IDP) that exists in two major isoforms, differentiated by the presence of three or four microtubule-binding repeats (3R or 4R). Both isoforms are found in approximately equal proportions in the brains of adult humans. Tau plays a critical role in stabilizing microtubules, which are essential components of the cytoskeleton responsible for maintaining cell shape, enabling intracellular transport, and supporting cell division. The microtubule-binding region (MTBR) of tau interacts with the interface between α- and β-tubulin heterodimers, facilitating microtubule polymerization, ensuring their stability, and promoting efficient axonal transport.[17,18]

*Tau in Disease*

There are over 80 phosphorylation sites on the longest isoform of tau (Figure 2b). Tau is phosphorylated in the physiological state, but its abnormal hyperphosphorylation may induce a conformational change that lowers its affinity for binding to microtubules.[17] Once detached, soluble tau oligomers form stacked β-sheet strands, which constitute the core of insoluble paired helical filaments (PHFs).[19] PHFs aggregate to form the insoluble neurofibrillary tangles (NFTs) characteristic of AD (Figure 2a).[20] This tau pathology contributes to neurotoxicity, disrupting intracellular transport and leading to neuronal degeneration.

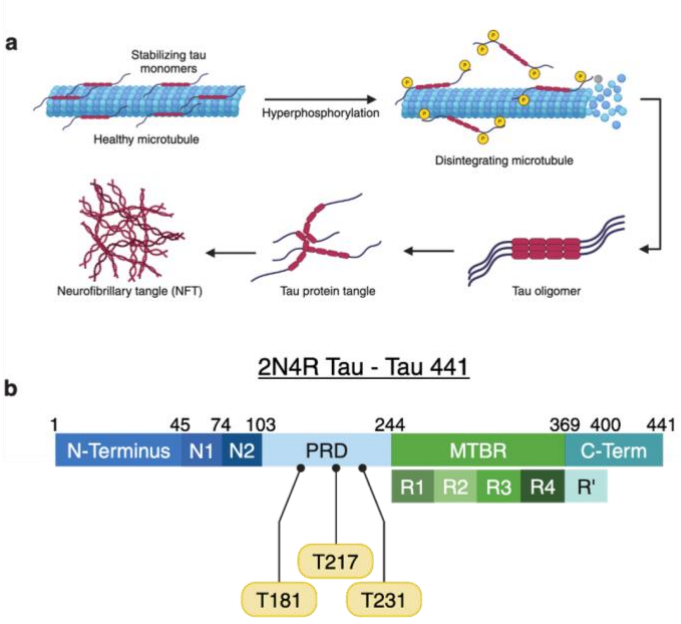


**Figure 2.** The hyperphosphorylation of tau leads to its aggregation into neurofibrillary tangles (NFTs). **a** Hyperphosphorylation of tau induces a conformational change that prevents it from binding and stabilizing the microtubules, leading to the formation of insoluble NFT pathology. **b** Full-length Tau (441 residues long) can be phosphorylated at over 80 serine, threonine, and tyrosine (STY) residues throughout the protein, with many phosphorylation sites in the proline-rich domain (PRD) strongly associated with Alzheimer's disease

Hyperphosphorylated tau is linked to a group of disorders known as tauopathies. Although these diseases exhibit diverse phenotypes and neuropathological features, they are classified together due to the common pattern of tau aggregation. Tauopathies include AD, progressive supranuclear palsy (PSP), corticobasal degeneration (CBD), Pick's disease (PiD), chronic traumatic

encephalopathy (CTE), and frontotemporal dementia with parkinsonism linked to chromosome-17 (FTDP-17).

Mutations in the MAPT gene, which encodes tau, promote tau aggregation. [21] Specifically, autosomal dominant mutations in MAPT have been linked to cases of FTDP-17, demonstrating that tau pathology alone can drive central nervous system degeneration.[22]

Tauopathies are classified in several ways. Firstly, they are characterized by their ratio of 3R to 4R tau isoforms and grouped into 3R, 4R, and 3R/4R tauopathies.[23] Additionally, they are divided into primary tauopathies, where tau is the major pathological component, and secondary tauopathies, where tau aggregation is considered a response to other pathological events.

Although it has been established that tau aggregation is sufficient to drive neurodegeneration, future work is required to further understand the impact of phosphorylation on the molecular mechanisms underlying disease progression. These tauopathies are linked by the abnormal accumulation of tau in the brain, but their clinical symptoms present differently. Comparing these tauopathies may reveal conserved, phosphorylation-dependent molecular mechanisms that contribute to neurodegeneration.

*Primary Age-Related Tauopathy (PART)*

However, tauopathy pathology is not limited to individuals with neurodegenerative diseases. Primary Age-Related Tauopathy (PART) is commonly observed in the brains of aging individuals, where neurofibrillary tangles (NFTs) are present, but without significant amyloid plaques, regardless of dementia status.[24] While many individuals with PART are cognitively normal and exhibit no significant cognitive impairment, some develop mild cognitive impairment or dementia, which correlates with the severity of tau pathology.[25] The neuropathology of PART closely resembles AD-associated NFTs, with both 3R and 4R tau isoforms present in the aggregates found in medial temporal lobe and other brain regions. Despite these similarities, PART differs

from AD in that NFT pathology does not extensively progress to neocortical regions, has a lesser impact on cognition, and patients generally have a longer lifespan.[26] While there is ongoing debate about whether PART is part of the continuum of AD-associated dementia progression, it can also coexist with other neurodegenerative conditions, including tangle-predominant senile dementia (TPSD), tangle-only dementia, preferential development of NFTs without senile plaques, and senile dementia of the neurofibrillary tangle type (SD-NFT).[27]

### 1.4 Alzheimer's Disease (AD)

*Overview*

Alois Alzheimer recorded the tauopathy case with his discovery of AD in 1906 through the autopsy of Auguste D., a female patient at the Frankfurt Psychiatric Hospital.[28] He observed her cognitive decline from its onset, linking memory disturbances to the histopathological features later defined as amyloid plaques and NFTs.

AD is the most common secondary tauopathy. Globally, the prevalence of AD and other dementias has increased by 160.84% between 1990 and 2019, increasing from 19.79 million cases to 51.62 million cases.[29] Accordingly, the number of deaths world-wide has tripled over the past 30 years, increasing from 0.56 million to 1.62 million.[29] The strongest risk factor for AD is advanced age, but cases of early onset AD may show symptoms before age 65. With prevalence and morbidity steadily increasing, the development of new methods to improve diagnosis and treatment is critical.

*Clinical Symptoms*

The National Institute of Neurological and Communicative Disorders and Stroke (NINCDS) and the Alzheimer's Disease and Related Disorders Association (ADRDA) established criteria for the diagnosis of AD in 1984 involving eight cognitive domains: memory, language, perceptual skills, attention, constructive abilities, orientation, problem solving and functional abilities.[30] The primary

clinical symptoms of AD include a progressive decline in episodic memory and cognitive function.[31] A typical amnesic presentation is marked by difficulties in acquiring and recalling new information. Patients may repeatedly ask the same questions, misplace personal belongings, or forget appointments. Additional symptoms include impairments in reasoning, judgment, visuospatial abilities, and language functions, along with personality and behavioral changes such as apathy, aggression, and depression.

*Neuropathology*

Extracellular deposits of amyloid-β plaques and neurofibrillary tangles of aggregated phosphorylated tau are significantly correlated to the presence of clinical AD (Figure 3). However, past studies have demonstrated that amyloid deposition is linked to cognitive impairment through NFT formation, leading to inflammation, synaptic impairment, and neuronal loss.[32] Recent *in vivo* studies supporting the amyloid cascade hypothesis suggest that amyloid-β promotes tau hyperphosphorylation and aggregation.[33] While amyloid-β and tau are widely believed to act together in driving Alzheimer's disease, the dual pathway hypothesis proposes that upstream factors independently trigger amyloid-β and tau pathologies.[32] Consequently, both amyloid-β and tau have been the targets of diagnostic testing and therapeutic development for AD.

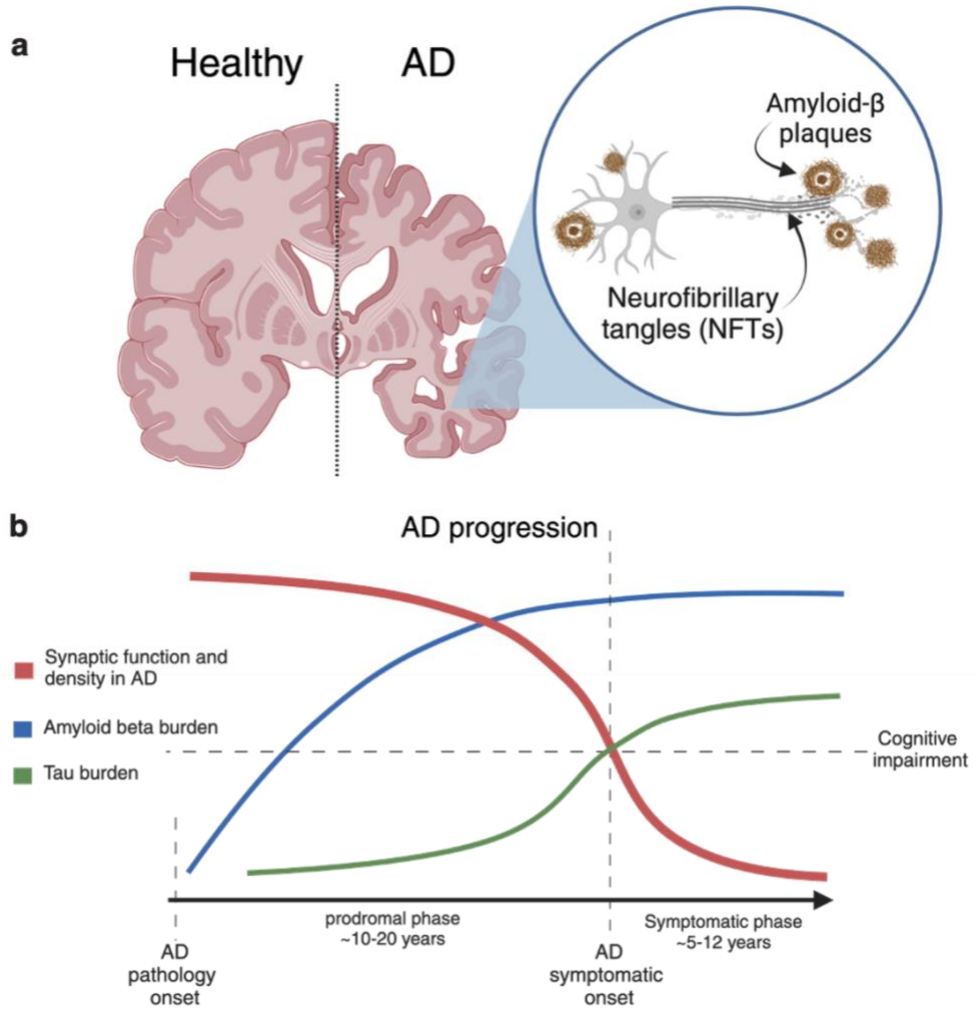


**Figure 3.** Alzheimer's disease overview.
**a** The two primary hallmarks of AD pathology are extracellular amyloid-β plaques and intracellular NFTs. **b** Theoretical model (Jack curve style) of disease progression over time where amyloid beta and tau burden correlate with decreased synaptic function and density and increased cognitive impariment.[34]

*Diagnosis*

Cognitive impairment in AD is diagnosed through a combination of patient history, input from a knowledgeable informant, and objective cognitive assessments, including mental status examinations and neuropsychological testing. While AD neuropathology has historically been confirmed by autopsy, modern diagnostic approaches integrate PET imaging, cerebrospinal fluid (CSF) and blood biomarkers, and neuropsychological testing to enable earlier detection.[35]

AD staging begins at the preclinical stage, where biomarkers are present in the absence of clinical symptoms.[31] Mild cognitive impairment (MCI) due to AD involves the presence of core clinical symptoms and AD probability is validated by biomarker tests. In the final stage, AD dementia, patients meet dementia criteria, exhibiting a gradual onset and progressive worsening of symptoms over time.

Recent studies have reported three defined stages of clinical AD diagnosis: preclinical, MCI, and dementia. Reflecting this, an "ABC" staging protocol was developed to classify AD neuropathologic changes based on Aβ/amyloid plaques (A), neurofibrillary tangles (NFTs) (B), and neuritic plaques (C). Amyloid pathology, extracellular deposits of the amyloid beta (Aβ), can be described by Thal phases of Aβ/amyloid plaques distribution on the brain. NFT pathology is determined by Braak staging, which describes abundance and location of NFT distribution within the brain. Neuritic plaques, extracellular deposits of Aβ peptides with a more complex morphology than amyloid plaques, are classified by the Consortium to Establish a Registry for AD (CERAD) neuritic plaque scoring system. Additionally, the impact of comorbid conditions, such as Lewy Body Disease and Vascular Brain Injury, on dementia symptoms in AD patients is increasingly recognized.

### 1.5 Frontotemporal Dementia with Parkinsonism Linked to Chromosome-17 (FTDP-17)

*Overview*

Atrophy of the frontal and temporal lobe was first described during the late 19th century by Arnold Pick, a German doctor whose observations initially classified the entire frontotemporal dementia (FTD) spectrum as Pick's disease (PiD).[36] However, discrepancies between the clinical and neuropathological definitions of PiD have led to the broader use of frontotemporal dementia (FTD) or frontotemporal lobar degeneration (FTLD).

FTLD-associated clinical syndromes occur in around 10 out of 100,000 people.[37] FTDP-17, also known as frontotemporal dementia with a microtubule-associated protein tau (MAPT) gene

mutation, was classified as a subtype of FTLD at the 1996 international consensus conference on FTD in Ann Arbor, Michigan.[38] It is a rare autosomal dominant disorder with an undetermined prevalence, identified in over 100 families worldwide with 38 unique genetic mutations.[39] P301L, N279K, and a splice site mutation (exon 10 +16) are the most common mutations, accounting for 60% of cases.[39] FTDP-17 is considered a familial subset of FTLD-tau, which is a type of frontotemporal lobar degeneration characterized by abnormal tau pathology in neurons and glia that includes both sporadic and genetic forms.

The P301L mutation on the MAPT gene was first detected in a Dutch family and U.S. family with frontotemporal dementia and parkinsonism in 1998.[22] This mutation affects only 4R tau, as it involves the substitution of proline with leucine at position 301 in exon 10, which is spliced out from 3R tau mRNA. Tau aggregates collected from the Unites States family were composed primarily of 4R tau, corresponding with the P301L mutation present on 4R tau in some cases of FTDP-17.[22] FTDP-17 linked to the P301L mutation is a 4R tauopathy and most tau mutations associated with FTDP-17 increase splicing of exon 10 and thus levels of 4R tau. However, some FTDP-17 mutations, such as the +19 and +29 intronic mutations close to the 5' spice site of exon 10, are associated with a higher percentage of 3R tau.[40]

*Clinical Symptoms*

FTDP-17 is part of a clinically and pathologically heterogeneous group of neurodegenerative diseases characterized by atrophy of the frontal and temporal lobes. The age of onset typically occurs around 50 years, with symptoms including personality and behavioral abnormalities, as well as dementia.[39] Patients often experience poor impulse control, apathy, psychosis, language difficulties, and impaired executive function. Memory deficits typically emerge later in disease progression. Parkinsonism-related motor symptoms, such as rigidity and bradykinesia, often develop, and progressive speech difficulties and seizures may also occur; however, resting tremors are uncommon.

*Neuropathology*

Despite the clinical and neuropathological heterogeneity observed with the condition, most patients experience atrophy of the frontal and temporal cortex, the basal ganglia, and substantia nigra.[41] Brain atrophy typically presents alongside filamentous deposits of hyperphosphorylated tau in neurons and glial cells, neuronal loss, and gliosis.[42] Lewy bodies and amyloid deposition have not been observed in this condition, while Pick bodies are only sometimes present.

*Diagnosis*

While there is not a strict set of criteria for the diagnosis of FTDP-17, a combination of clinical and pathological features alongside molecular genetic analysis is used.[39] Patients typically develop at least one of the following neurological symptoms between the third and fifth decade: behavioral and personality disturbances, motor dysfunction, or cognitive deficits. Additionally, patients are likely to have a family history of the disease. Imaging studies such as computerized tomography (CT) and magnetic resonance imaging (MRI) are often used to exclude other diagnostic possibilities such as a brain tumor, abscess, multi-infarct state, or hydrocephalus. Biofluid tests are usually negative, and electroencephalography (EEG) are typically normal, especially early in the disease. FTDP-17 is often misdiagnosed as PiD, PSP, or CBD in cases where there is no positive family history. Therefore, neuropathological analysis and molecular genetic testing of the tau gene are essential for accurately differentiating these conditions.

### 1.6 Progressive Supranuclear Palsy (PSP)

*Overview*

PSP was first described in 1964 by Steele as a progressive brain disease characterized by supranuclear ophthalmoplegia, or muscle weakness causing the loss of control over the vertical gaze, dysarthria, or muscle weakness causing difficulty speaking, and neck and upper body muscle rigidity.[43] It is a rare disease with a prevalence of about 5-7 cases per 100,000 people, with symptoms typically presenting in a person's mid to late 60s.[37] Richardson's Syndrome (PSP-

RD) is the most well characterized muscular phenotype of PSP.[44] However, there are other PSP phenotypes that are less well characterized, so the prevalence of PSP syndromes may be higher than previously estimated.

*Clinical Symptoms*

Progressive Supranuclear Palsy (PSP) encompasses a range of clinical phenotypes characterized by behavioral, language, and movement abnormalities linked to tau protein aggregation. Symptoms of PSP-Richardson Syndrome (PSP-RS) include balance issues, unsteady gait, bradykinesia, subtle personality changes, cognitive slowing, executive dysfunction, speech difficulties, and impaired ocular movement. PSP-parkinsonism (PSP-P) has a slower disease progression compared to PSP-RS and often presents with tremor, bradykinesia, and rigidity resembling Parkinson's Disease (PD). Progressive Supranuclear Palsy with Progressive Gait Freezing (PSP-PGF) presents as an isolated gait disorder before the development of PSP-RS symptoms. While the clinical presentation of PSP often overlaps with Corticobasal Degeneration (CBD), particularly with progressive asymmetrical limb apraxia, parkinsonism, dystonia, and specific cognitive impairments, post-mortem analysis can differentiate PSP-related corticobasal syndrome from CBD. PSP-speech language (PSP-SL) involves difficulty with grammar and halting speech, often preceding the development of PSP-RS. PSP with frontal presentation (PSP-F) is marked by early and progressive deterioration in personality, social behavior, and cognition. Finally, PSP with predominant cerebellar ataxia (PSP-C) presents with cerebellar ataxia, or poor muscle coordination, prior to the development of PSP-RS.

*Neuropathology*

PSP is a primary 4R tauopathy, where tau aggregates in both neurons and glial cells. Neuropathological characterization of PSP requires Neuropathological characterization of PSP requires the presence of NFTs or neuropil threads of aggregated tau protein in the basal ganglia and brainstem.[45] Tau pathology in PSP progresses from subcortical regions to the cerebellar and

cortical areas of the brain. Additionally, neuronal loss, gliosis, tufted astrocytes, and oligodendroglial coiled bodies are observed in affected regions.

*Diagnosis*

PSP is diagnosed clinically by clinicopathological correlations, where diagnoses are typically made three to four years after the first presentation of symptoms. The National Institute of Neurological Disorders and Stroke (NINDS) and the Society for PSP, Inc. (SPSP) established three stage criteria to determine PSP diagnosis certainty in 1996: possible PSP, probable PSP, and definite PSP. However, these criteria are biased towards PSP-RS, the most common phenotype. So, a new clinical diagnoses paradigm called the International Parkinson and Movement Disorder Society (MDS-PSP) Criteria was proposed in 2017 to expand upon the NINDS criteria and facilitate earlier and more accurate PSP diagnosis.[46]

PSP is a sporadic disease according MDS-PSP criteria, so routine genetic testing is not utilized for diagnosis. The minimum age of diagnosis is 40 years old and the four core functional domains for diagnosis include ocular motor dysfunction, postural instability, akinesia, and cognitive dysfunction. However, neuropathological is required for definite PSP diagnosis based on morphological and biochemical characteristics.

Additionally, PSP diagnosis is challenging due to its overlap with PD in its early stages. Alternate differential diagnoses include CBD, FTD, and AD and these conditions must be ruled out. MRIs are used to scan the brain to exclude additional alternative diagnoses such as extensive small vessel disease, leukodystrophy, normal pressure hydrocephalus and frontal mass lesions.

### 1.7 Why study phosphorylation?

Investigating the phosphoproteome provides insight into disease-specific phosphorylation patterns on tau and other proteins, helping to uncover altered signaling pathways, potential biomarkers, and therapeutic targets. Since phosphorylation is a key regulator of cellular

processes, comparing AD, FTDP-17, and PSP can identify disrupted kinase and phosphatase networks, shedding light on why tau pathology manifests differently across these disorders despite their shared aggregation pathology. Beyond tau, other phosphoproteins involved in cytoskeletal stability, synaptic function, and neuroinflammation may also contribute to disease progression. Given the diagnostic challenges of FTDP-17 and PSP, identifying distinct phosphorylation signatures in brain tissue and, eventually, biofluids could improve differential diagnosis and early detection. Additionally, understanding these phosphorylation networks may inform the development of targeted kinase inhibitors, phosphatase modulators, or other pathway-specific interventions tailored to each disease. Ultimately, phosphoproteomic analyses can refine diagnostic tools and therapeutic strategies, improving our ability to combat these neurodegenerative disorders.

*Diagnosis*

Current diagnostic measures for neurodegenerative diseases are often invasive (e.g., cerebrospinal fluid analysis), expensive (e.g., neuroimaging), and time-consuming (e.g., neuropsychological assessments).[47] These challenges are compounded by the overlap in clinical symptoms and neuropathological features among tauopathies, as well as the diverse phenotypic presentations of these diseases, making accurate diagnosis difficult.[48] This underscores the urgent need for more specific and accessible tools to differentiate AD from other tauopathies.

One significant advancement in this area is the use of positron emission tomography (PET) to measure amyloid-β and tau pathologies in AD patients using radioactive tracers. In 2020, the first PET tracer capable of detecting aggregated tau neurofibrillary tangles in adults with cognitive impairment under evaluation for AD—18F-flortaucipir (AV1451)—was approved.[49] While amyloid-β PET tracers had previously been developed, 18F-flortaucipir marked a major breakthrough in visualizing tau aggregation *in vivo*. This tracer is particularly valuable for differential diagnosis, as a negative 18F-flortaucipir scan can help rule out AD as the cause of dementia.[50]

However, PET imaging has limitations: it is costly, requires specialized personnel and facilities, and can only capture one pathological marker at a time.[51] Furthermore, PET tracers for non-AD tauopathies are still underdeveloped. This gap in diagnostic tools has driven ongoing research into cerebrospinal fluid (CSF) and plasma biomarkers that can stage AD and potentially distinguish it from other tauopathies.

Current studies focus on biomarkers such as Aβ42, total tau (t-tau), and phosphorylated tau (p-tau) to better understand hyperphosphorylation's role in neurodegenerative disease and improve diagnostic accuracy.[52] P-tau181 is a well-established AD biomarker, but recent findings suggest that the CSF p-tau217/tau217 ratio correlates more strongly with amyloid and tau PET imaging and clinical measures of AD.[53] Moreover, elevated CSF p-tau231 levels emerge earlier in disease progression, preceding global amyloid PET positivity.[54] Furthermore, tau phosphorylated at residues 181, 217, and 231 in plasma has been shown to differentiate AD from non-AD neurodegenerative disorders.[55]

*Treatment*

Aducanumab and Lecanemab are monoclonal antibodies that target amyloid beta (Aβ) and have demonstrated clinically significant reductions in amyloid plaques, leading to their approval for early AD treatment.[56,57] However, emerging research suggests that tau pathology correlates more strongly with cognitive decline than amyloid burden, driving the development of anti-tau therapeutics. These therapies could not only advance AD treatment but also offer insights into other tauopathies.

The hyperactivation of glycogen synthase kinase-3 (GSK-3) is hypothesized to contribute to tau hyperphosphorylation in AD. Current studies have demonstrated that treating triple-transgenic AD mice models with GSK-3β inhibitors significantly lowered levels of hyperphosphorylated tau.[58] Another key kinase, cyclin-dependent kinase 5 (CDK5), also phosphorylates tau, and the CDK5

inhibitory peptide (CIP) has been shown to suppress aberrant tau phosphorylation in cortical neurons under neurotoxic conditions, highlighting CDK5 as a potential therapeutic target.[59] Since phosphatase activity is diminished in AD, enhancing phosphatase function may offer an alternative treatment approach. For example, increasing the activity of $Mg^{2+}/Mn^{2+}$ dependent 1A (PPM1A) by NPLC0393, a compound isolated from *Gynostemma pentaphyllum*, improved cognitive impairment in triple transgenic AD mice by repressing tau hyperphosphorylation.[60]

While no anti-tau therapeutics have been FDA-approved for AD treatment, a deeper understanding of the mechanisms driving tau hyperphosphorylation in AD and related tauopathies could reveal new therapeutic targets.

### 1.8 How to study phosphorylation?

*Immunoassays*

Immunoassays are the primary method for detecting abnormally phosphorylated proteins, with common techniques including immunohistochemistry, enzyme-linked immunosorbent assays (ELISA) and western blots. Immunohistochemical (IHC) staining with a monoclonal antibody specific for tau, PHF-tau or specific p-tau phosphosites is the standard method used as the primary method to detect tau pathology in brain tissue.[49,61] IHC allows both for the visualization and localization of the target antigen, which in this case is PHF-tau. The sandwich ELISA is often used to detect p-tau in CSF and plasma, in a similar manner to IHC. In this technique, a monoclonal capturing antibody specific for phosphorylated tau is applied to the biological sample.[62] Then, a reporter antibody and a chemiluminescent secondary substrate are applied to visualize the p-tau. Simoa (SIngle MOlecule Array) digital ELISA immunoassays also quantify tau phosphorylated at specific different phosphosites in CSF and plasma. For this method, magnetic beads are conjugated to a capture antibody specific for p-tau 217.[63] A biotinylated reporter is then added, allowing fluorescence imaging to quantify p-tau217.

Similar immunoassays have been employed to compare levels of p-tau181, p-tau217, and p-tau231, helping to validate CSF and plasma biomarkers for AD. Developing methods to distinguish tau phosphorylated at different sites is crucial, as certain p-tau variants may be more effective in differentiating AD from other tauopathies.[64] For example, CSF p-tau217 correlates better with PET tracer [$^{18}$F]flortaucipir than p-tau181, indicating it may be a stronger biomarker of AD.[65] Additionally, p-tau231 levels appear to increase earlier than p-tau181, suggesting that the early detection of soluble tau in plasma could be critical for diagnosing AD in its initial stages.[66]

While antibody-based assays have enabled the quantification of low concentrations of phosphorylated proteins, they come with several limitations. The quality of results depends on the availability of antibodies with a high affinity for the protein of interest, and the cost of immunoassay kits has risen in recent years. Furthermore, many of these methods can only identify one protein at a time. To address these challenges, recent developments have enabled the use of mass spectrometry to identify tau and other phosphorylated proteins implicated in disease through multiplexing, which allows the quantification of multiple analytes in a single run. This reduces sample processing time and enables a more complete characterization of AD biomarkers.

However, the use of mass spectrometry assays requires further development and optimization to achieve accuracy and specificity in phosphoprotein identification. For example, a study comparing diagnostic performance of antibody-free mass spectrometry determined that p-tau217 and p-tau231 were comparable immunoassay methods, but p-tau181 quantified using mass spectrometry had inferior diagnostic performance and lower association with amyloid-PET and tau-PET.[67] Building upon these findings, the use of mass spectrometry to identify biomarkers to differentiate AD from other tauopathies requires further development.

*Proteomics*

Proteomics is the large-scale study of proteins using liquid chromatography-tandem mass spectrometry (LC-MS/MS) (Figure 4a). The first step in this method is tissue homogenization,

which disrupts cell membranes and extracellular structures to release proteins into stabilizing buffer solutions. Given the complexity of protein structures, they are then enzymatically digested into smaller peptides using proteases like trypsin, improving separation, specificity, and sensitivity during LC-MS/MS analysis. During LC-MS/MS, peptides are ionized and separated based on their mass-to-charge ratio (m/z) within the mass spectrometer. The resulting spectra display detected peptide masses, which are matched to known protein sequences.

Phosphoproteomics allows for the use of mass spectrometry to identify proteins from these pathways to identify biomarkers and therapeutic targets. Phosphorylation, the addition of a phosphate group ($PO_4^{3-}$), increases a peptide's mass by 79.9663 Da. By analyzing fragmentation patterns of modified and unmodified peptides, mass spectrometry can pinpoint the exact phosphorylation sites on tau, providing crucial insights into disease-associated modifications. However, the study of phosphoproteins is often difficult due to their low abundance and co-existence with their non-phosphorylated isoforms in the cell. To address this limitation, phosphorylation enrichment strategies are employed to enhance sensitivity in the mass spectrometry detection and quantification of phosphoproteins from human brain tissue.[68] Methods for enrichment include immobilized metal-affinity chromatography (IMAC) enrichment with metal oxides (e.g. $Fe^{3+}$,$TiO_2$, $ZrO_2$), cation and anion exchange chromatography, antibody capture, chemical derivation, and calcium phosphate precipitation.[69]

Fe-IMAC is the most widely tested method to isolate phosphoproteins, which uses a positively charged $Fe^{3+}$ chromatography matrix to bind negatively charged phosphate groups (Figure 4b).[70] Phosphoproteins can be enriched at the peptide or protein level to remove non-phosphorylated proteins or peptides. Since peptides have less complex structure than proteins, it is beneficial to digest samples with Trypsin and Lys-C prior to enrichment to promote binding specificity. While peptide-level enrichment improves the likelihood that lower abundance proteins will be identified,

limitations arise because protein identification now relies on a single phosphopeptide, and the molecular weight and isoelectric point of the proteins cannot be observed. Previous studies conducted by our group identified 2% of the total brain proteome as phosphopeptides, whereas 71% of the proteome consisted of phosphopeptides after IMAC enrichment.[34]

After IMAC enrichment, phosphopeptides are identified by liquid chromatography-mass spectrometry (LC-MS). For this study, the Evosep One will be used for purification and separation prior to identification and quantification by the TimsTOF HT mass spectrometer. Developed by Bruker Daltonics, the TimsTOF HT mass spectrometer couples Trapped Ion Mobility Spectrometry (TIMS) with Quadrupole Time-of-Flight (TOF) mass spectrometry to identify peptides based on mobility separation and mass/charge separation.[71] The addition of TIMS introduces an additional layer of selectivity based on mass, charge, and shape when separating ions, improving peak capacity and reducing the complexity of the mass spectra. Data-dependent acquisition (DDA) will be utilized to obtain higher resolution of the production spectra of the precursor ions with the greatest mass-to-charge (m/z) signal intensity. While DDA may lose the signal from low abundance proteins, its increased sensitivity is beneficial for targeted analysis of peptides in an existing database.

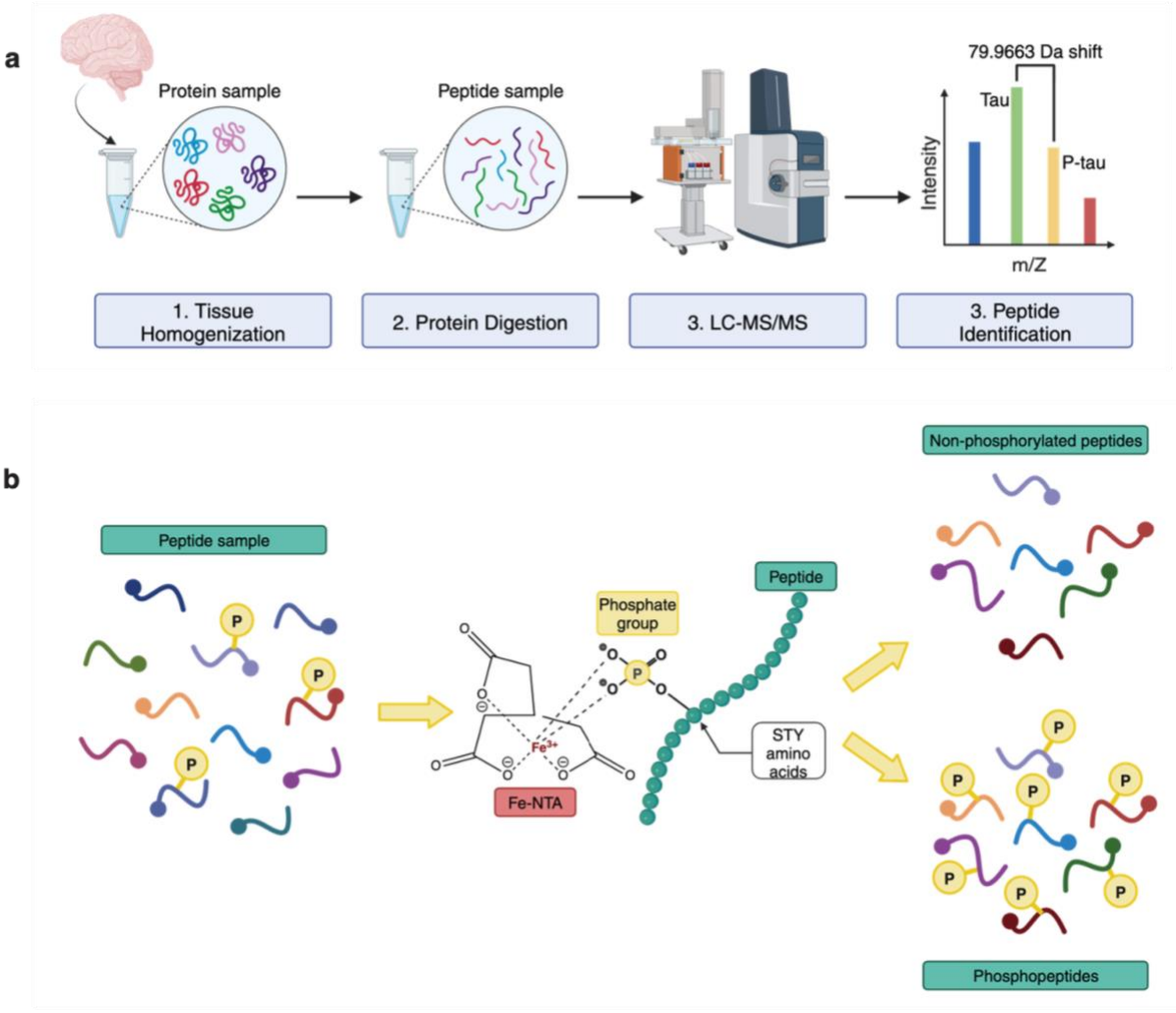


**Figure 4.** Study of phosphorylated proteins using proteomics.
**a** Proteomics pipeline to study the brain tissue proteome involves tissue homogenization, protein digestion, liquid chromatography-tandem mass spectrometry, and peptide identification. **b** The addition of a Fe-IMAC phosphopeptide enrichment step after the protein digestion and before LC-MS/MS can improve the detection of phosphopeptides by removing non-phosphorylated peptides.

## 1.9 Hypothesis and Specific Aims

*Hypothesis*

Further research is needed to clarify the role of specific tau phosphorylation sites in AD, particularly in their potential as diagnostic biomarkers and therapeutic targets. Comparisons of site-specific tau phosphorylation across different tauopathy conditions remain limited, despite their importance for differential diagnosis. A broader understanding of phosphoproteins beyond tau is also essential, as other phosphorylated proteins may contribute to disease pathology and serve as novel biomarkers or therapeutic targets. Identifying and characterizing previously

unrecognized phosphopeptides could provide new avenues for improving diagnosis and treatment strategies across neurodegenerative disorders.

This study will investigate the phosphoproteins relevant to AD and related tauopathies compared to non-demented control samples, and how these proteins correlate with disease-specific alterations in phosphorylation-dependent signaling pathways. This question will be addressed through the development of a sensitive and specific LC-MS/MS method for the identification and quantification of low-abundance phosphopeptides associated with tauopathies (Figure 5).

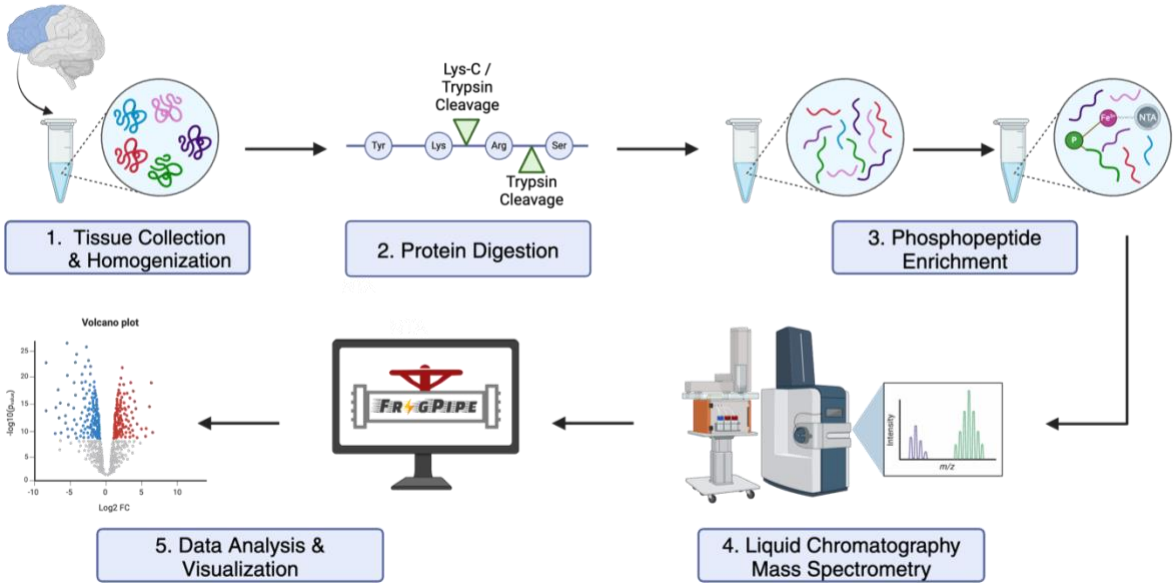


**Figure 5.** Experimental overview of phosphoproteomic pipeline involving a protease digestion of homogenized brain tissue with Lys-C and trypsin, phosphopeptide enrichment by Fe-NTA IMAC, and proteomic analysis by DDA LC-MS/MS.

I hypothesize that the development of a sensitive and specific Fe-IMAC LC-MS/MS method for the identification and quantification of low-abundance phosphopeptides will further inform our understanding of site-specific phosphorylation in neurodegenerative disease and uncover disease-specific dysregulation of protein phosphorylation pathways (Figure 5). Gaining a deeper understanding of the molecular mechanisms underlying AD, FTDP-17, and PSP will help clarify the pathological differences between these diseases, which are often grouped together due to

their shared tau-related pathology. Additionally, identifying the factors responsible for tau hyperphosphorylation may uncover commonalities across these conditions, highlighting the significance of investigating kinase and phosphatase profiles in each unique disease state.

This investigation will establish validity by comparing findings with canonical phosphopeptides implicated in AD, with a focus on proteins modified at canonical serine, threonine, and tyrosine (STY) phosphosites. Tau, encoded by the MAPT gene, is the most well-characterized protein hyperphosphorylated in AD brains and tubulin is the most well-known interactor of tau.[72] MAP1A and MAP2 are also extensively phosphorylated in AD.[69] Additional phosphoproteins known to be associated with tau are neurofilaments, MAP1B, and CRMP2.[68] Building on existing knowledge of the AD phosphoproteome, this study aims to develop methods to identify novel pathways and proteins affected by aberrant phosphorylation in tauopathies. This advancement will deepen our understanding of disease mechanisms, enhance biomarker discovery and early diagnostic potential, and inform the development of targeted therapies.

*Aim 1: Establishing Viability of Fe-IMAC Phosphopeptide Enrichment for Brain Tissue Analysis*

An in-house Fe-IMAC protocol will be optimized for phosphopeptide enrichment from brain tissue. As a proof-of-concept, the method will be applied to AD and control brain samples, followed by LC-MS/MS analysis. Raw data will be processed using FragPipe to identify phosphoproteins, impute missing values, and perform statistical analyses to determine differentially enriched proteins and gene ontology groups.

*Aim 2: Enhancing Fe-IMAC Sensitivity and Reproducibility for Phosphoproteomics*

Experimental conditions for Fe-IMAC enrichment and LC-MS/MS will be refined to maximize phosphoproteome depth and coverage. Parameters such as starting protein concentration, incubation times, and Fe-NTA bead recharging will be optimized to enhance sensitivity and reproducibility in AD brain tissue.

*Aim 3: Comparative Phosphoproteomic Analysis of AD and Related Tauopathies*

Using the optimized workflow from Aims 1 and 2, phosphoproteomic profiles of AD, FTDP-17, PSP, and non-demented controls will be analyzed. Comparative analyses will identify disease-specific and shared phosphorylation patterns across tauopathies.

## Chapter 2: Aim 1: Development of Fe-IMAC Phosphopeptide Enrichment for Brain Tissue

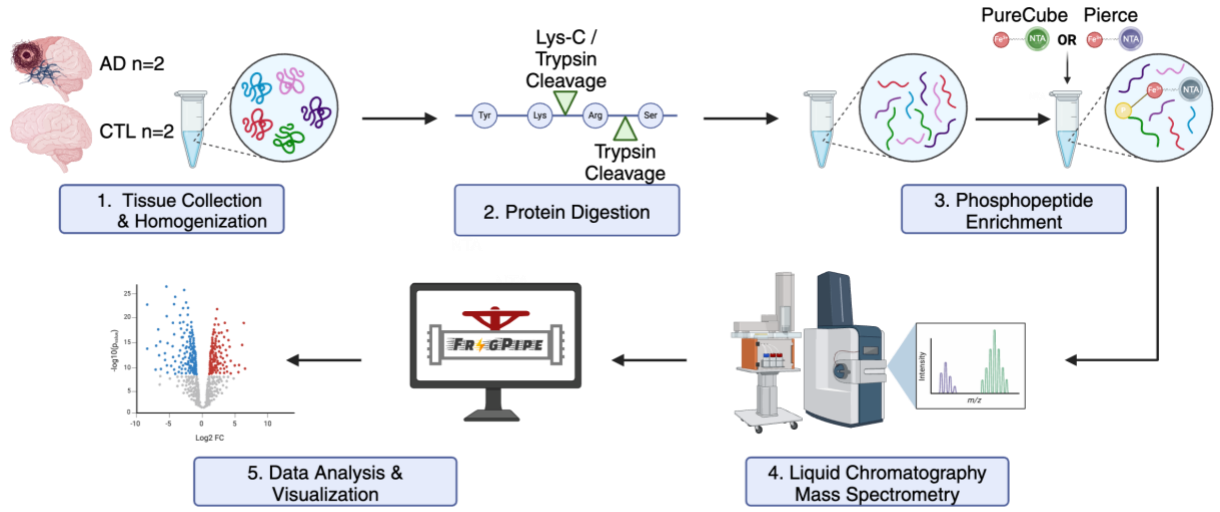


**Figure 6.** Experimental workflow for Aim 1: Development of Fe-IMAC phosphopeptide enrichment for brain tissue.

### 2.1 Methods

*2.1.1 Brain Tissue Homogenization*

Postmortem frozen human brain of AD and non-demented control sections of the frontal cortex were obtained from the Emory Alzheimer's Disease Research Center Brain Bank (pathological traits described in Table 1). AD and control samples were age and sex matched as closely as possible. The AD case was pathologically confirmed by Braak Stage VI determination and Consortium to Establish a Registry for Alzheimer's Disease (CERAD) level 3, whereas the control case was Braak Stage 0 and CERAD level 0.

Brain tissue samples were homogenized as described.[74,75] Approximately 150-200 mg of brain tissue was homogenized in NP-40 lysis buffer ( 50mM Tris-HCl (pH 7.4), 150mM NaCl, 1%NP-40 and 5mM EDTA) and protease and phosphatase inhibitors (HALT) with ≈100 µL stainless-steel beads (0.9 to 2.0 mm NextAdvance) by a bullet blender minutes twice at 4ºC for 3 minute intervals. Lysates were then centrifuged at 3,000 x g at 4ºC for 30 seconds. Supernatant was

collected and added to 400 μL of lysis buffer before centrifugation at 10,000 x g for 10 min. The top 2 layers were collected, and protein concentration was measured using a bicinchoninic acid (BCA) assay (Pierce).

**Table 1.** Pathological traits for human brain tissues used to establish viability of Fe-IMAC phosphopeptide enrichment for brain tissue analysis.

| Case Number | Primary Neuropathologic Diagnosis | Notes | Braak Stage | ABC | CERAD | Post Mortem Interval (hr) | Age at Onset | Age at Death/Bx | Duration (years) | ApoE | Race | Sex |
|---|---|---|---|---|---|---|---|---|---|---|---|---|
| OS98-11 | AD | NA | VI | 3 | 3 | 6 | 56 | 65 | 9 | E4/4 | w | f |
| E05-130 | Control | PART | 0 | 1 | 0 | 3 | NA | 52 | NA | E3/4 | w | f |

*2.1.2 Protease Digestion*

To digest AD and control brain tissue samples, 1,100 μg of protein per sample was normalized to 4 μg/μL in Tris-HCl (pH 8.0) buffer. Lysates were reduced with 5 mM dithiothreitol (DTT) and alkylated with 10 mM iodoacetamide (IAA) at room temperature for 30 minutes, respectively. Then, the proteins were diluted 1:1 v/v in 100 mM Tris-HCl (pH 8.0). Proteins were digested overnight at room temperature at a 1:25 ratio of Lys-C protease (Thermo Fisher) to protein. Then, Trypsin Protease (Thermo Fisher) was added at a ratio of 1:25 Trypsin to protein and incubated overnight. The following day, enzyme activity was quenched with acidifying buffer [1:9, v/v; 10% formic acid (FA) and 1% trifluoroacetic acid (TFA)] and desalted by loading the peptides onto a 10 mg Oasis PRiME HLB 96-well plate (Waters), washing twice with 0.1% TFA and then eluting with 50% acetonitrile (ACN) and 0.1% TFA. Desalted peptides were dried down with a CentriVap Centrifugal Vacuum Concentrator (Labconco) overnight.

*2.1.3 Fe-NTA Magnetic Bead Preparation*

Fe-Nitrilotriacetic acid (NTA) magnetic beads were prepared by washing and recharging Ni-NTA magnetic beads with $FeCl_3$. Thermo Scientific™ Pierce™ Ni-NTA Magnetic Agarose Beads (78606) and PureCube Ni-NTA MagBeads (31201) were compared for specificity and sensitivity. After the storage solution was removed using a magnetic test tube rack, the beads were washed 3 times

with 1 mL high performance liquid chromatography water (HPLC-$H_2O$) and vortexed in between each wash. 1 mL of 40 mM EDTA (Invitrogen) was then added, and the beads were vortexed for 30 minutes. The beads were washed another 3 times with 1 mL HPLC-$H_2O$. 1 mL of 100 mM $FeCl_3$ (Carolina) was added, and the beads were vortexed for 2 hours. The beads were then washed with 1 mL of a 1:1:1 solution of ACN, methanol (MeOH), and 0.01% acetic acid in HPLC-$H_2O$ and vortexed. Next, the beads were washed three times with 80% ACN + 0.1% TFA (Binding Buffer) and stored in 1 mL Binding Buffer.

*2.1.4 Phosphopeptide Enrichment*

Peptides were resuspended in Binding Buffer in $H_2O$ to give a final concentration of 1 μg/μL. 100 μg of protein were collected for mass spectrometry as the input to record the total proteome. 500 μg of AD and control peptides were combined with activated Pierce or PureCube magnetic beads, respectively. To normalize the binding capacity, 25 μL of the PureCube beads in a 25% suspension and 28.57μL of the Pierce beads in a 25% suspension were used per 500 μg of protein. Samples were vortexed for 30 minutes to allow the phosphopeptides to bind to the Fe-NTA magnetic beads and the supernatant was collected to observe non-binding proteins. Proteins were eluted from beads with 50% ACN and 2.5% $NH_4OH$, and vortexed intermittently for 1 minute. Samples were centrifuged at 14,000 rpm for 1 minute and then the beads were washed another 3 times with 1 mL MPA. The samples were then acidified with 100 μL of 50% ACN + 5% FA and then dried down. The beads were washed twice in 1 mL HPLC-$H_2O$ and 40 mM EDTA was added before vortexing for 5 minutes. The beads were washed another 3 times in in 1 mL HPLC-$H_2O$, resuspended in 20% MeOH, and stored at 4ºC for reuse.

*2.1.5 Liquid Chromatography – Tandem Mass Spectrometry (LC-MS/MS)*

The samples were reconstituted using in mass spectrometry grade water + 0.1% FA to give a concentration of 1 μg/μL, before diluting further to a concentration of 200 ng/μg. 20 μL from each sample was deposited onto Evosep tips, prepared according to manufacturer's instructions, and inserted in the Evosep tray. Samples loaded onto Evotip trap columns were separated in a 44-min gradient (30 samples per day) on an EV-113 Performance column with the Evosep One system (EV-1000, Evosep, Denmark). Peptide separation was conducted at 40°C with 35% 0.1% FA in ACN (Mobile phase B, MPB) at flow rate of 500 nL/min. Detection of the peptides was performed on a TimsTOF HT (Bruker, Bremen, Germany) in DDA-PASEF short-gradient positive-ion mode, with a mass range of 100-1700 m/z, ion mobility range of 0.85-1.3 V*s/cm$^2$, cycle time of 0.5 s and a ramp time of 100 ms.

*2.1.6 Database Search and Quantification*

Raw files were searched with FragPipe (v 22.0) essentially as described.[76] The proteins were identified by searching against the 06 June 2024 canonical Human Uniprot database with APOE2, APOE, and ABeta40/42 with 40,808 entries and 20,004 decoys. The default FragPipe Label-Free Quantitation – Match Between Runs (LFQ-MBR) workflow was loaded with default parameters with minimal modifications. Fragpipe relies upon MSFragger (v 54.1) for database searching and peptides identification. Precursor mass tolerance was -20 to 20 ppm, fragment mass tolerance of 20 ppm, with mass calibration and parameter optimization selected, and isotope error was set to 0/1/2. Enzyme specificity was set to strict-trypsin with up to 2 missed cleavages allowed. Peptide length ranged from 7 to 50 amino acids, and peptide mass from 500 to 5,000 Da. Variable modifications included: methionine oxidation (+15.9949 Da), N-terminal acetylation (+42.0106 Da), and phosphorylation on STY residues (+79.96633 Da) with a maximum of 3 variable

modifications per peptide. Fixed modification included cysteine carbamidomethylation (+57.02146 Da). Peptide-to-spectra matches were rescored with MSBooster and Percolator for predicting retention time and spectra with a minimum probability of 0.5. Percolator (v 3.6.4) filtered peptide spectral matches (PSMs) using a support vector machine algorithm to control PSMs matched to peptides from decoy proteins. MaxLFQ values were determined through IonQuant (v 1.1027). The parameters were as follows: 2 minimum MaxLFQ ions, match between runs (MBR), MBR ion False Discovery Rate (FDR) of 0.01, normalize intensity across runs, and peptide-protein uniqueness was unique+razor. Additional parameters included 3 minimum scans, 2 minimum isotopes, an m/z tolerance of 10 ppm, a retention time tolerance of 0.4 min, and an IM tolerance of 0.05 1/k0. MBR RT tolerance was 1 minute, IM tolerance was 0.05 1/k0, MBR peptide FDR was 1, MBR min correlation was 0, MBR top runs was 10, and MBR protein FDR was 1.

*2.1.7 Differential Abundance, Ontological Enrichment, and Data Visualization*

Proteins absent in 50% or more of the samples were removed and the remaining proteins were retained for downstream analyses. A Perseus Style imputation was performed using an in-house function in R (Version 2023.12.1+402) to impute missing values. Values were imputed according to a noise level -1.8SD from the mean of the log2(LFQ abundance) values and a normal distribution where values fall +/-0.3SD from noise level was assumed. Differentially expressed proteins were identified by a one-way ANOVA and no false discovery rate (FDR) correction was implemented. Significantly altered proteins with corresponding log10 unadjusted p-values were represented as volcano plots generated with the ggplot2 package in R, which can be found at https://www.github.com/edammer/parANOVA. BaderLab's monthly updated ontology lists were used to implement a Fisher Exact Test for enrichment $p<0.05$ and 5 minimum genes per ontology determine genes of Fe-IMAC enriched proteins using the GOparallel function in R, which can be found at https://www.github.com/edammer/GOparallel.

## 2.2 Results

Phosphoproteomics enables the investigation of phosphorylation patterns in proteins, offering insight into dysregulated kinase- and phosphatase-dependent signaling pathways in AD. However, studying phosphoproteins is challenging due to their low abundance and the presence of non-phosphorylated isoforms. To enhance the detection of phosphopeptides and maximize phosphoproteome coverage in AD brain tissue, an Fe-IMAC enrichment protocol was developed and optimized (Figure 6).

This phosphopeptide enrichment methods relies on the use of magnetic agarose beads, which can be charged with $FeCl_3$ for the enrichment step. As such, the specificity for phosphopeptides of PureCube magnetic beads with a binding capacity of 80mg protein/1mL beads and Pierce magnetic beads with a binding capacity of 70mg protein/1mL beads were compared. Only 3% of the proteins detected in the input were phosphorylated, further demonstrating the importance of the phosphopeptide enrichment step to observe low-abundant phosphopeptides (Figure 6b). More proteins, peptides, and phosphopeptides were captured using the PureCube beads across all experimental groups (Figure 7a). Furthermore, all groups detected a higher percentage of phosphopeptides after the enrichment than before (Figure 7c). Additionally, the percentage of phosphopeptides was greater for the PureCube beads across all groups, with 25% and 56% phosphopeptides detected in the control and AD samples, respectively, compared to the 8% and 19% captured by the Pierce beads (Figure 7c). Additionally, the PureCube beads detected more unique phosphopeptides compared to the Pierce beads across all groups (Figure 7d). This data indicates that the PureCube beads will be the preferred agarose beads for future experiments.

Finally, the applicability of this protocol was applied to AD and non-demented control samples to determine the biological validity of this approach. Higher percentages of phosphopeptides and more unique peptides were observed in the AD samples across all groups (Figures 7d).

Additionally, one-way ANOVA revealed that 23 peptides were increased, and 31 peptides were decreased in the AD groups, indicating the role hyperphosphorylation may play in AD (Figure 7f). MAPT, the gene that encodes tau, was significantly increased in the AD group as expected, along with MAP1B and other proteins implicated in phosphorylation along the microtubule. Additionally, the intensity values for specific phosphorylated tau residues were compared between input and enriched AD samples (Figure 7e). Signals for T205 and T217 were lost after enrichment, whereas T50, SS195, and S404 were detected only in the enriched samples, not in the input. These findings suggest that this method can uncover phosphosites that may be undetectable in the total proteome but requires further refinement.

a

| Sample Group | Disease State | Total Proteins | Total Peptides | Peptides | Phosphopeptides | % Phosphopeptides |
|---|---|---|---|---|---|---|
| Input | Control | 2016 | 5940 | 5756 | 184 | 3.10% |
| | AD | 1647 | 4881 | 4742 | 139 | 2.85% |
| PureCube Enrichment | Control | 311 | 489 | 367 | 122 | 24.95% |
| | AD | 265 | 365 | 160 | 205 | 56.16% |
| Pierce Enrichment | Control | 190 | 259 | 238 | 21 | 8.11% |
| | AD | 237 | 296 | 240 | 56 | 18.92% |

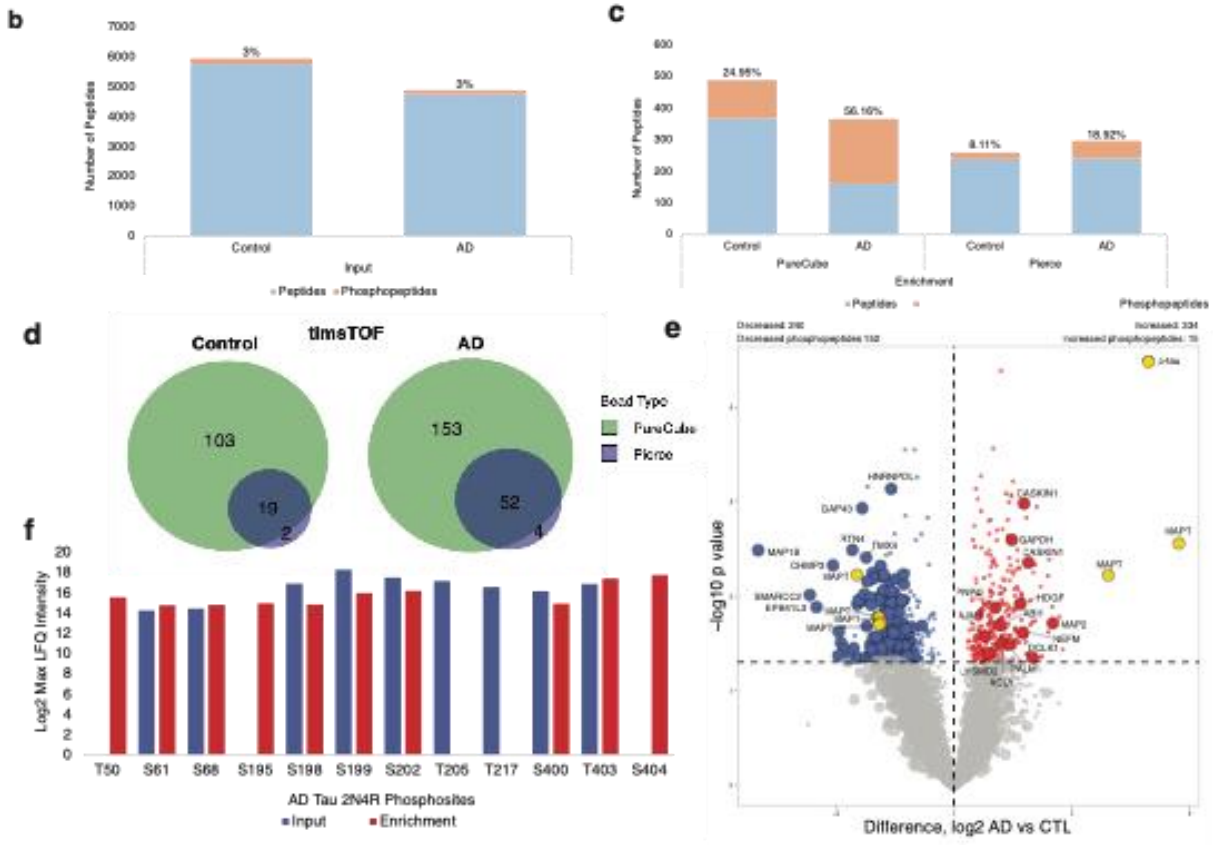

**Figure 7.** Preliminary stage optimization of phosphopeptide enrichment protocol.
**a** Proteins, peptides, and phosphopeptides from AD and non-demented brain tissue control samples were identified and quantified by FragPipe. The total proteome was collected prior to phosphopeptide enrichment by IMAC and IMAC results were compared between the PureCube and Pierce magnetic agarose beads. Phosphopeptides were determined by filtering the Fragpipe data for the phosphorylation PTM, which is a +79.9663 Dalton mass difference on the STY amino acids. **b** The percentage of phosphopeptides detected by LC-MS/MS from the total proteome before enrichment. **c** The percentage of phosphopeptides detected by LC-MS/MS from after enrichment using both the PureCube and the Pierce magnetic beads during IMAC. **d** Venn diagram of total proteins enriched by Fe-IMAC with PureCube and Pierce magnetic agarose beads detected by the TimsTOF HT. **e** The Log2 Max LFQ intensity, or relative protein abundance, is reported for each of the phosphosites detected after mapping to 2N4R tau. Phosphosites detected in the input are reported in red and phosphosites detected after enrichment using the PureCube beads are reported in purple. **f** Volcano plot displays IMAC enriched peptides detected by mass spectrometry by grouping the PureCube and Pierce enrichments as technical replicates to compare AD (n=2) to control (n=2). The Log2 Fold Change between AD and control groups is plotted on the x-axis while the –Log10 unadjusted p-value determined by one-way ANOVA is plotted on the y-axis. Peptides with $p < 0.05$ ($-\text{Log10} > 1.3$) are significant and highlighted and significant phosphopeptides are labeled.

## Chapter 3: Aim 2: Enhancing Fe-IMAC Sensitivity and Reproducibility for Phosphoproteomics

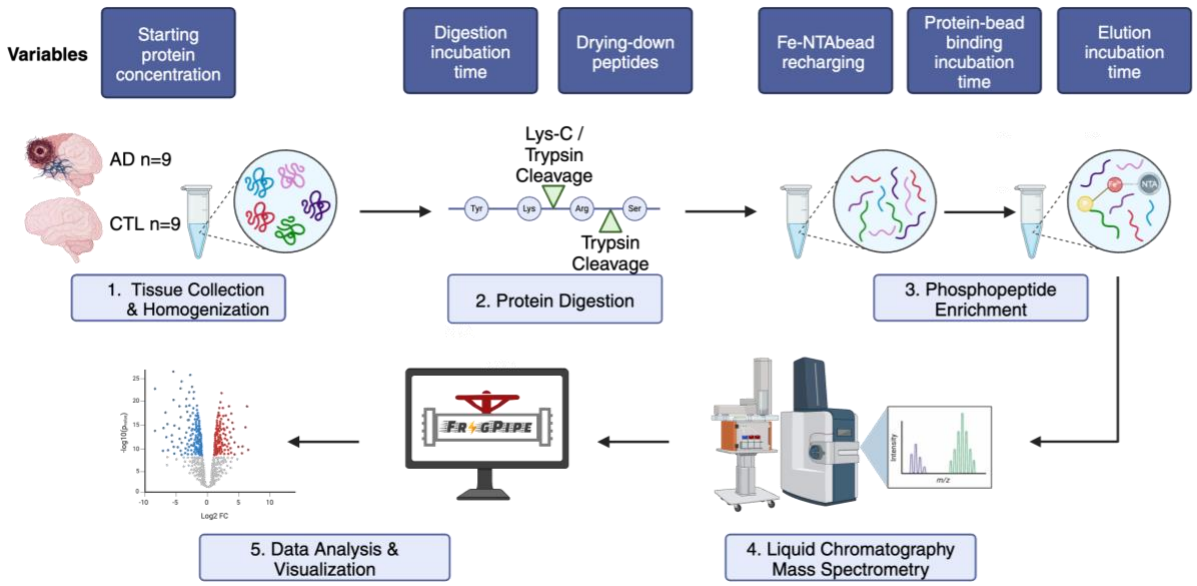


**Figure 8.** Experimental workflow for Aim 2: Enhancing Fe-IMAC Sensitivity and Reproducibility for Phosphoproteomics.

### 3.1 Methods

#### *3.1.1 Brain tissue homogenization*

Brain tissue was homogenized following protocol used in section 2.1.1. Postmortem frozen human brain of Alzheimer's Disease and non-demented control sections of the frontal cortex were obtained from the Emory Alzheimer's Disease Research Center Brain Bank (pathological traits described in Table 2).

**Table 2.** Pathological traits for human brain tissues used to enhance the Fe-IMAC sensitivity and reproducibility for phosphoproteomics.

| Case Number | Primary Neuropathologic Diagnosis | Notes | Braak Stage | ABC | CERAD | Post Mortem Interval (hr) | Age at Onset | Age at Death/Bx | Duration (years) | ApoE | Race | Sex |
|---|---|---|---|---|---|---|---|---|---|---|---|---|
| OS03-163 | AD | NA | VI | 3 | 3 | 4.5 | 52 | 55 | 3 | E3/4 | white | female |
| E08-101 | Control | PART | II | 0 | 0 | 11.5 | NA | 78 | NA | E3/3 | white | female |

#### *3.1.2 Protease Digestion*

500 μg of brain tissue for each condition being tested was normalized to 4 μg/μL in Tris-HCL pH 7.5 buffer. Each sample was digested with modifications made according to the experimental

variable being tested (Table 3). Final RAD (reduce, alkylate, denature) buffer concentrations were 100 mM TEAB, 1% Deoxycholate, 5 mM TCEP. RAD buffer was added to 250 μg, 500 μg, or 1,000 μg of AD and control samples at a ratio of 1μL RAD buffer to 10 μL sample and samples were vortexed and incubated for 10 minutes at 95ºC. Samples were cooled for 10 minutes at room temperature. LysC was added at a ratio of 1:100 LysC to protein and trypsin was added at a ratio of 1:10 trypsin to protein at the same time. Samples were vortexed and incubated for 1 hour, 4 hours, or overnight 37ºC. Formic acid was added to a final concentration of 0.5% to acidify each sample and samples were left to rest at room temperature for 20 minutes and then centrifuged at 16,000 x g for 10 minutes to pellet sodium deoxycholate.

Samples were cleaned up using Oasis Plate HLB 30 mg. The columns were activated with methanol, equilibrated with 0.1% TFA twice, and samples were loaded with 0.1% TFA. Samples were washed twice with 0.1% TFA and eluted twice with MPA. Samples were either dried down or stored at 4ºC.

**Table 3.** Experimental conditions for technical replicates

| *Variable* | *Sample Type* | *Starting Protein Amount (ug)* | *Digestion Time* | *Post Clean-up Dry Down* | *Binding Time* | *Bead Type* | *Elution Time* |
|---|---|---|---|---|---|---|---|
| *CTL* | | | | | | | |
| *Standard Protocol* | Control | 500 | ON (16 hours) | Yes | 30 min | Recharged | 1 min |
| *Starting Protein Amount* | Control | 250 | ON (16 hours) | Yes | 30 min | Recharged | 1 min |
| *Starting Protein Amount* | Control | 1000 | ON (16 hours) | Yes | 30 min | Recharged | 1 min |
| *Digestion Time* | Control | 500 | 1 hour | Yes | 30 min | Recharged | 1 min |
| *Digestion Time* | Control | 500 | 4 hours | Yes | 30 min | Recharged | 1 min |
| *Post Clean-up Dry Down* | Control | 500 | ON (16 hours) | No | 30 min | Recharged | 1 min |
| *Binding Time* | Control | 500 | ON (16 hours) | Yes | 2 hours | Recharged | 1 min |
| *Fe-NTA Beads* | Control | 500 | ON (16 hours) | Yes | 30 min | New Beads | 1 min |
| *Elution Time* | Control | 500 | ON (16 hours) | Yes | 30 min | Recharged | 30 min |
| *AD* | | | | | | | |
| *Standard Protocol* | AD | 500 | ON (16 hours) | Yes | 30 min | Recharged | 1 min |
| *Starting Protein Amount* | AD | 250 | ON (16 hours) | Yes | 30 min | Recharged | 1 min |
| *Starting Protein Amount* | AD | 1000 | ON (16 hours) | Yes | 30 min | Recharged | 1 min |
| *Digestion Time* | AD | 500 | 1 hour | Yes | 30 min | Recharged | 1 min |
| *Digestion Time* | AD | 500 | 4 hours | Yes | 30 min | Recharged | 1 min |
| *Post Clean-up Dry Down* | AD | 500 | ON (16 hours) | No | 30 min | Recharged | 1 min |
| *Binding Time* | AD | 500 | ON (16 hours) | Yes | 2 hours | Recharged | 1 min |
| *Fe-NTA Beads* | AD | 500 | ON (16 hours) | Yes | 30 min | New Beads | 1 min |
| *Elution Time* | AD | 500 | ON (16 hours) | Yes | 30 min | Recharged | 30 min |

### *3.1.3 Fe-NTA Magnetic Bead Preparation*

Fe-NTA magnetic beads were prepared by washing and recharging Ni-NTA magnetic beads. After the storage solution was removed using a magnetic test tube rack, the beads were washed 3 times with 1mL nanopure and vortexed in between each wash. 1 mL of 40 mM EDTA was then added and beads were rotated for 30 minutes. Beads were washed another 3 times with 1mL $H_2O$. Beads were washed once with 1 mL 10 mM $FeCl_3$, resuspended in 1 mL 10 mM $FeCl_3$ and left to rotate for 30 minutes. Beads were washed 3 times with $H_2O$ and equilibrated 3 times with MPA and stored in 125 μL of 1mL Binding Buffer to give a 5% bead suspension.

*3.1.4 Phosphopeptide Enrichment*

Peptides were resuspended in 125 μL Binding Buffer to give a final concentration of 4 μg/μL. AD and control peptides were combined with activated recharged magnetic beads from 1.1.5 or Fe-NTA PureCube beads at a ratio of 1 μL beads to 80 μL protein. Samples were rotated for 30 minutes or 2 hours to allow the phosphopeptides to bind to the Fe-NTA magnetic beads and the supernatant was saved. Beads were washed 3 times with Binding Buffer. Proteins were eluted from beads with 50% ACN and 2.5% $NH_4OH$, vortexed intermittently for 1 minute or 30 minutes, and acidified with 75% ACN + 10% FA. Samples were dried down. Beads were washed with 1 mL 50% ACN, 50% MeOH, and 0.01% acetic acid and stored in the same buffer at 4ºC before being washed and recharged for future use.

*3.1.5 Liquid Chromatography – Tandem Mass Spectrometry (LC-MS/MS)*

The samples were reconstituted using 500 μ L μL of 0.1% FA in water for the flow through (total proteome) and were diluted to of 25 μg / μL with of 0.1% FA in water. The eluted samples were reconstituted in 200 μL of 0.1% FA in (assumed 1% recovery according to Cube Biotech protocol). 20 μL was loaded onto EvoSep tips in triplicate, resulting in 500 ng protein per tip. LC-MS/MS was run following protocol from section 1.2.5.

*3.1.6 Database Search and Quantification*

Data was searched and quantified following protocol from section 2.1.6.

*3.1.7 Differential Abundance, Ontological Enrichment, and Data Visualization*

Differential Abundance, ontological Enrichment, and data visualization were performed according to section 2.1.7.

## 2.2 Results

The first attempt to enrich phosphopeptides in brain tissue achieved varying levels of success, with the percentage of phosphopeptides present post enrichment ranging from 8% to 77% (Figure 6c). However, success of the enrichment cannot be evaluated based on the percentage of phosphopeptides detected alone, for the depth of the proteome coverage must be considered. Between 16 and 281 phosphopeptides were identified per enrichment, suggesting that further work is required to optimize the protocol to increase the number of peptides detected. To achieve this goal, several parameters were evaluated for their impact on the proteome depth and sensitivity: starting protein concentration, trypsin/LysC digestion incubation time, post-digestion drying down, protein-bead binding incubation time, recharging of the beads with $FeCl_3$, and elution incubation time (Figure 8-9a). Comparing the relative intensities of tau peptides phosphorylated at specific amino acids revealed that the phosphoenrichment step enables the detection of phosphosites not captured in the input proteome (Figure 9b). The biological implications of this method were evaluated by comparing the AD and control samples, demonstrating that phosphorylated tau is significantly increased in AD and further establishing the validity of this method to detect phosphorylated tau and other disease-relevant phosphoproteins (Figure 9c).

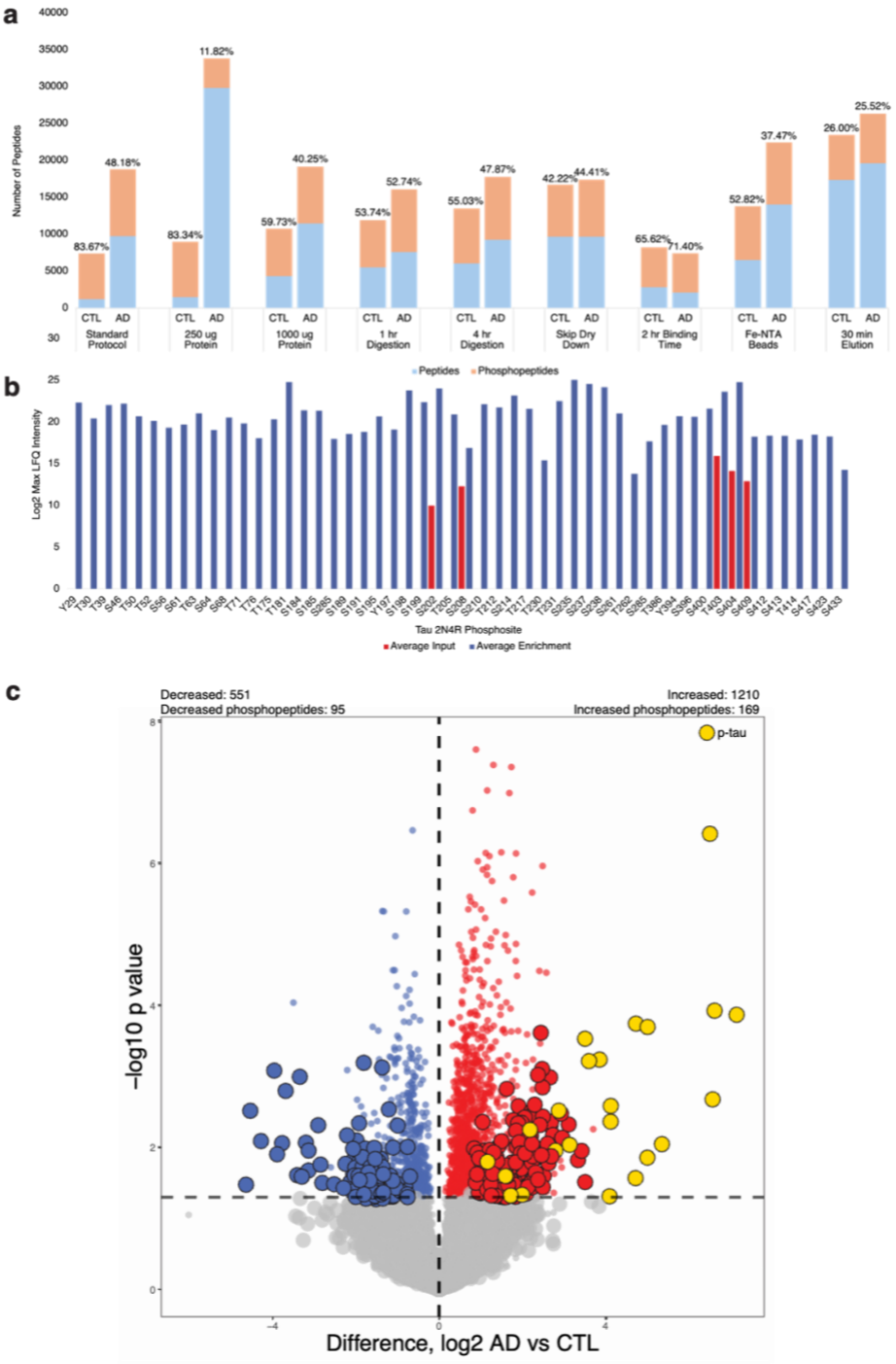


**Figure 9.** Depth and sensitivity of phosphopeptide enrichment in brain tissue.
**a** The standard protocol serves as a baseline for comparison because it closely follows the protocol utilized in the pilot experiment, where 500 mg of protein was used, the digestion incubation was overnight, the peptides were dried down between the digestion and the enrichment, the bead:protein binding time was 30 minutes, the Ni-NTA beads were recharged with $FeCl_3$ prior to enrichment, and the elution was 1 minutes. Starting concentrations of 500mg, 250 mg, and 1000mg were compared to determine how much protein is required to achieve phosphopeptide enrichment. Overnight, 1 hour, and 4 hour digestion times were compared. The peptides were not dried down following the digestion to observe if this preserved phosphate interactions. The protein suspensions were left on the beads for 2 hours to

incubate to observe the impact on binding specificity. Fe-NTA PureCube beads were used to observe if the recharging of Ni-NTA beads with Fe-Cl was successful. The beads were left in elution buffer for 1 or 30 minutes prior to collection of the eluate. **b** The Log2 Max LFQ intensity, or relative protein abundance, for the average the AD (n=9) and control (n=9) technical replicates for each phosphosite detected mapped to 2N4R tau. Phosphosites detected in the input are reported in red and phosphosites detected after enrichment are reported in purple. **c** Volcano plot shows that the phosphoenrichment successfully enriches phosphorylated MAPT in AD samples. The Log2 Fold Change between the AD (n=9) and control (n=9) technical replicates was plotted on the x-axis while the –Log10 unadjusted p-value determined by one-way ANOVA is plotted on the y-axis. Peptides with $p < 0.05$ ($–\text{Log10} > 1.3$) are significant and highlighted, with significant phosphopeptides being enlarged and phosphorylated tau (MAPT) being enlarged and highlighted in yellow.

## Chapter 4: Aim 3: Comparative Phosphoproteomic Analysis of AD and Related Tauopathies

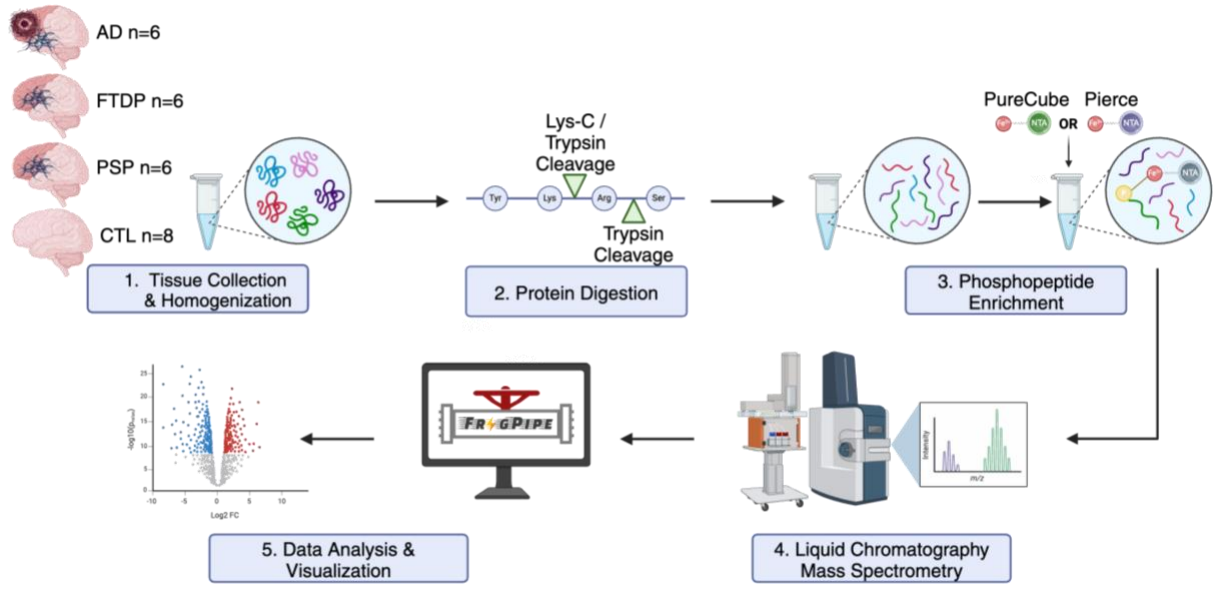


**Figure 10.** Experimental workflow for Aim 3: Comparative Phosphoproteomic Analysis of AD and Related.

### 4.1 Methods

*4.1.1 Brain Tissue Homogenization*

Brain tissue was homogenized following protocol used in section 2.1.1. Postmortem frozen human brain of AD, FTDP-17, PSP, and non-demented control sections of the frontal cortex were obtained from the Emory Alzheimer's Disease Research Center Brain Bank (pathological traits described in Table 4). 6 AD samples, 6 FTDP-17 samples, 6 PSP samples. And 8 control samples were used for this study. Since only a subset of FTDP-17 samples were confirmed to have the P301L mutation, they will henceforth be referred to as FTDP.

**Table 4.** Pathological traits used for comparative phosphoproteomic analysis of AD and related tauopathies.

| Case Number | Primary Neuropathologic Diagnosis | Notes | Braak Stage | ABC | CERAD | Post Mortem Interval (hr) | Age at Onset | Age at Death/Bx | Duration (years) | ApoE | Race | Sex |
|---|---|---|---|---|---|---|---|---|---|---|---|---|
| *OS98-11* | AD | NA | VI | 3 | 3 | 6 | 56 | 65 | 9 | E4/4 | w | f |
| *OS00-32* | AD | NA | VI | 3 | 3 | 3.5 | 55 | 62 | 7 | E3/4 | w | m |
| *E08-53* | AD | NA | VI | 3 | 3 | 8 | 70 | 78 | 10 | E3/3 | w | f |
| *OS00-12* | AD | NA | V | 3 | 3 | 6 | 69 | 72 | 3 | E3/4 | w | m |
| *OS03-163* | AD | NA | VI | 3 | 3 | 4.5 | 52 | 55 | 3 | E3/4 | w | f |
| *E05-04* | AD | NA | VI | 3 | 3 | 4.5 | 51 | 64 | 13 | E3/4 | w | f |
| *OS98-06* | FTDP-17 | P301L | na | 0 | 0 | 5 | 59 | 63 | 4 | E3/3 | w | m |
| *E08-24* | FTDP-17 | P301L | 0 |  | 0 | 7 | 56 | 64 | 8.5 | E3/4 | w | m |
| *E10-32* | FTDP-17 | unclassified | III | 2 | 2 | 18 | 81 | 89 | 8 | E3/3 | w | f |
| *E12-70* | FTDP-17 | CBD; PSP | II | 1 | 0 | 5 | 66 | 69 | 3 | E3/3 | w | m |
| *E12-152* | FTDP-17 | unclassified | VI | 3 | 2 | 11.5 | 80 | 89 | 9 | E2/4 | w | m |
| *E15-84* | FTDP-17 | unclassified | na | NA | 3 | 12 | 68 | 75 | 7.5 | NA | w | f |
| *OS00-33* | PSP | FTLD-tau | III | 1 | 0 | 11.5 | 74 | 82 | 8 | E2/3 | w | f |
| *E13-113* | PSP | MCI | III | 1 | 0 | 10 | 70 | 83 | 13 | E3/3 | w | m |
| *OS97-07* | PSP | FTLD-tau | I | 0 | 0 | 3 | 51 | 61 | 10 | NA | w | m |
| *E07-151* | PSP | FTLD-tau | II | 1 | 3 | 10 | 65 | 75 | 10 | E3/4 | w | m |
| *E10-48* | PSP | FTLD-tau | IV | 2 | 3 | 14 | 89 | 94 | 5 | E3/3 | w | f |
| *E17-152* | PSP | FTLD-tau; CBD-features | na | NA | 0 | 11 | 70 | 75 | 5 | NA | w | m |
| *E05-130* | Control | PART | 0 | 1 | 0 | 3 | NA | 52 | NA | E3/4 | w | f |
| *E08-101* | Control | PART | II | 0 | 0 | 11.5 | NA | 78 | NA | E3/3 | w | f |
| *OS02-35* | Control | PART | I |  | 0 | 6 | NA | 75 | NA | E3/3 | w | f |
| *E06-41* | Control | PART | II |  | 0 | 10 | NA | 57 | NA | E3/3 | w | m |
| *A86-85* | Control | NA | na | NA | NA | 6 | NA | 58 | NA | E3/3 | w | m |
| *OS03-380* | Control | PART | II | 1 | 0 | 12 | NA | 61 | NA | E3/4 | b | m |
| *E16-45* | Control | PART | I | 1 | 0 | 2.5 | NA | 70 | NA | E3/3 | b | m |
| *E20-18* | Control | PART | I | 0 | 0 | 7 | NA | 72 | NA | E3/3 | w | m |

### *4.1.2 Protease Digestion*

600 μg of brain tissue for each sample for each condition was digested according to the standard protocol section 3.1.2.

### *4.1.3 Fe-NTA Magnetic Bead Preparation*

Fe- Nitrilotriacetic acid (NTA) magnetic beads from Cube Biotech were used. Beads were equilibrated three times with MPA and stored in 125 μL of 1mL Binding Buffer to give a 5% bead suspension.

### *4.1.4 Phosphopeptide Enrichment*

Peptides were resuspended in 150 μL of Binding Buffer to give a final concentration of 4 μg/μL. 100 μg of protein were collected for mass spectrometry to observe the total proteome. The

remaining 500 μg from each sample was combined with activated Fe-NTA PureCube magnetic beads at a ratio of 1 μL beads to 80 μL protein. Samples were rotated for 30 mins to allow the phosphopeptides to bind to the Fe-NTA magnetic beads and the supernatant was saved. Beads were washed 3 times with Binding Buffer. Proteins were eluted from beads with 50% ACN and 2.5% $NH_4OH$, vortexed intermittently for 1 minute, and acidified with 75% ACN + 10% FA. Samples were dried down. Beads were washed with 1 mL 50% ACN, 50% MeOH, and 0.01% acetic acid and stored in the same buffer at 4ºC before being washed and recharged for future use.

*4.1.5 Liquid Chromatography – Tandem Mass Spectrometry (LC-MS/MS)*

The total proteome samples were reconstituted using 100 uL of MPA and were diluted to of 25 μg / uL with of MPA in water. The eluted samples were reconstituted in 200 μL of MPA (assumed 1% recovery). The flow through samples were reconstituted using 500 uL of MPA and were diluted to of 25 μg/μL with 0.1% FA in water. 20 μL was loaded onto EvoSep tips in triplicate, resulting in 500 ng protein per tip. Global pooled standards for each group (total, enrichment, flow through) were created by mixing the diluted samples for each of the respective groups in equal proportions and loading 20 μL onto EvoSep tips. Samples were run on Evosep coupled with TimsTOF HT at 30 SPD.

*4.1.6 Database Search and Quantification*

Data was searched and quantified following protocol from section 2.1.6.

*4.1.7 Differential Abundance and Ontological Enrichment*

Differential Abundance, ontological enrichment, and data visualization were performed according to section 2.1.7. To visualize the disease-relevant proteins, the ANOVAout files for AD, FTDP, and PSP versus control were merged, LFQ intensities were normalized by z-score and scaled to transform the data ranges from -4 to +4. The resulting matrix was visualized in R using the

ComplexHeatmap library. The software BioVenn was used to construct venn diagrams comparing significant phosphopeptides across diseases.

### 4.2 Results

The phosphoenrichment protocol optimized in the second aim of this project was applied to 8 control samples, 6 Alzheimer's disease (AD) samples, 6 frontotemporal dementia with Parkinsonism (FTDP) samples, and 6 progressive supranuclear palsy (PSP) samples to examine conserved and distinct phosphoproteins across these tauopathies (Figure 10). Prior to LC-MS/MS analysis, Coomassie blue staining and western blotting were conducted to assess the presence of phosphorylated tau (p-tau) in the brain tissue lysates (Figure 11d). These analyses revealed that p-tau was predominantly found in the AD samples, with varying levels in the control, FTDP, and PSP samples. While tau aggregation is a common feature in all tauopathies, tau hyperphosphorylation was most severe in AD.

Before comparing the phosphoproteomes across tauopathies, the success of the phosphoenrichment was first validated by comparing the enrichment proteomes to the input proteomes for the AD samples (Figure 11). A plot of AD versus control data comparing the input and enrichment data sets revealed a low biweight midcorrelation of 0.28, suggesting a significant change in protein intensities after enrichment (Figure 11b). Moreover, comparing the peptides present in both the enrichment and input data sets demonstrated that more phosphopeptides were present at higher intensities in the enrichment samples than in the input samples, with phosphorylated tau being significantly enriched in the latter (Figure 11b). This indicates that the enrichment strategy effectively increased the detection of phosphoproteins, particularly low abundance phosphopeptides. However, variability was observed in the total number of peptides detected, as well as the percentage of phosphopeptides detected, both within and across disease

groups (Figure 11c). This variability may contribute to inconsistencies in the detection of phosphopeptides.

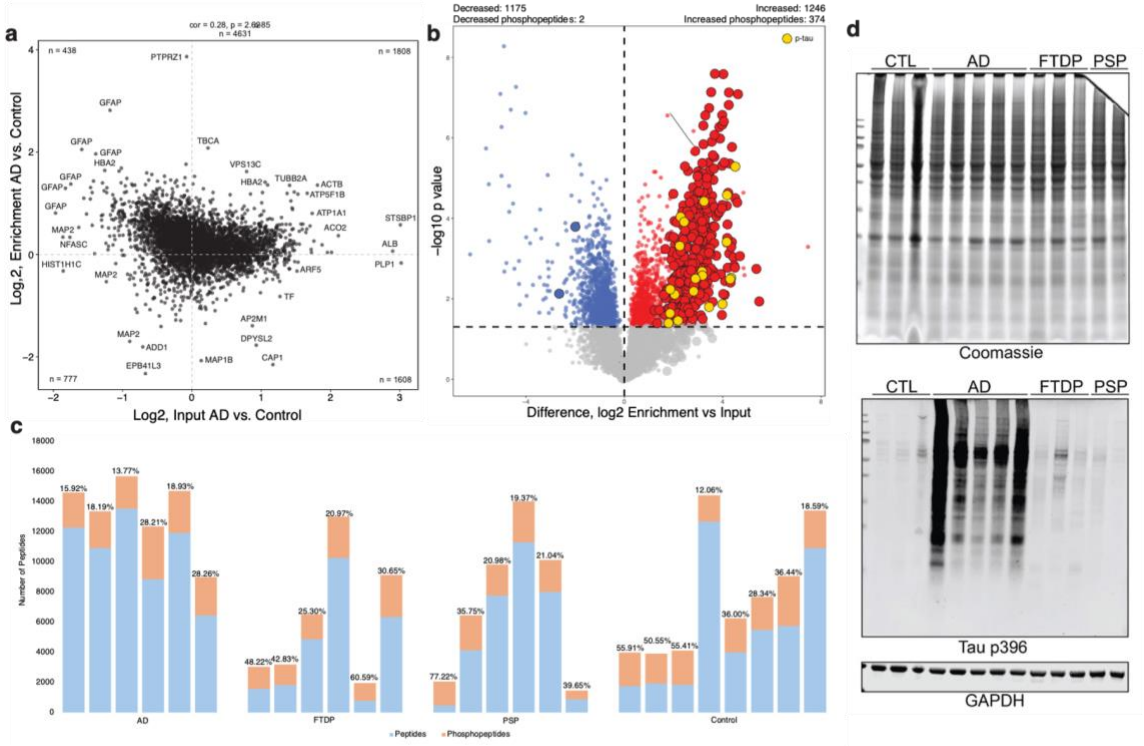


**Figure 11.** Quality control for tauopathy comparison enrichment.
**a** A scatter plot illustrates the correlation between $log_2$ fold-change (AD vs CTL) of significantly altered proteins in the input and enrichment data sets. There are 4,631 overlapping proteins overlapping in the two sets with a low degree of biweight midcorrelation (*bicor* = 0.28, $p < 2.62e^{-85}$). **b** Mass spectrometry identified 374 significant phosphopeptides compared to 2 in inputs. Volcano plot displays the Log2 Fold Change between groups plotted on the x-axis while –Log10 unadjusted p-value, as determined by one-way ANOVA, is plotted on the y-axis. A $p < 0.05$ (-Log10 = 1.3) was employed for stringency to identify significantly enriched peptides. Enlarged points indicate significant phosphopeptides and yellow enlarged points indicate phosphorylated tau. **c** The percentage of phosphopeptides detected by LC-MS/MS from the AD, FTDP, PSP, and control proteomes after enrichment. **d** Coomassie blue stain demonstrated equal protein concentrations for each lysate. Western blotting revealed tau p396 was increased in AD compared to CTL, FTDP, and PSP samples, with GAPDH serving as a loading control.

The log2 fold change of the AD versus control peptides was plotted against the -log10 p value for each peptide, revealing the significant peptides and phosphopeptides relevant to the pathological state (Figure 12a). The same comparison was made for FTDP and PSP (Figure 12b-c). Interestingly, more phosphopeptides were significantly decreased than increased in AD, despite the hyperphosphorylation that occurs in the pathological state. As expected, several isoforms of

tau, including pT217, pT231, and pT235, were significantly altered in AD. Notably, MAPT pT217 was decreased in FTDP, and MAPT pT231 was decreased in PSP, highlighting distinct phosphorylation changes in these tauopathies.

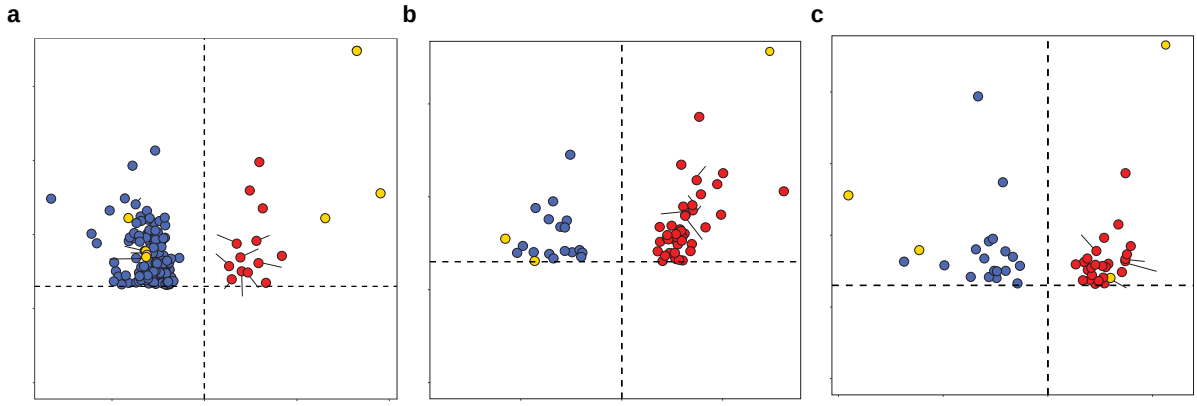


**Figure 12.** Phosphoenrichment reveals differences in phosphoproteomes across AD, FTDP, and PSP.
Volcano plots display IMAC enriched peptides in **a** AD vs CTL, **b** FTDP vs CTL, and **c** PSP vs CTL. The Log2 Fold Change between each respective tauopathy and control groups is plotted on the x-axis while the –Log10 unadjusted p-value determined by one-way ANOVA is plotted on the y-axis. Peptides with $p < 0.05$ (–Log10 > 1.3) are significant and highlighted, with significant phosphopeptides being enlarged.

The functions of the genes identified through this phosphoproteomic pipeline were examined (Figure 13). Significant proteins relevant to each disease were clustered and annotated by mapping them against gene lists to describe their functions in the cell. For example, phosphatase binding was increased in AD, which may reflect a cellular attempt to counteract hyperphosphorylation (Figure 13a). Additionally, tau binding was decreased in AD, despite the accumulation of tau (Figure 13d). GO terms related to cytoskeleton structure and organization were decreased in AD, FTDP, and PSP (Figure 13d-f), aligning with tau's role in stabilizing microtubules. Furthermore, GO terms involving protein polymerization and refolding were increased in AD, FTDP, and PSP, suggesting that tau and other proteins may be struggling to maintain their proper structure in these pathological states.

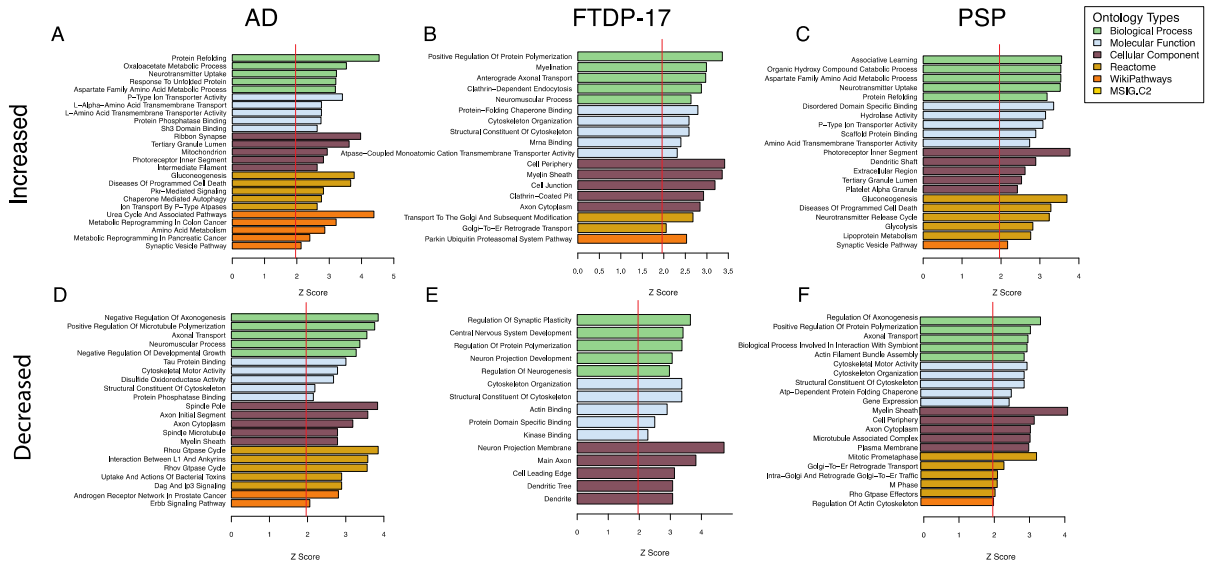


**Figure 13.** Top Gene Ontology (GO) terms for each tauopathy versus control.
Fisher Exact Test for enrichment p<0.05 was used to map gene lists onto Biological Process, Molecular Function, Cellular Component, Reactome, WikiPathways, and MSIG.C2 gene lists. **a-c** GO terms increased in AD, FTDP, and PSP versus control, respectively. **d-f** GO terms decreased in AD, FTDP, and PSP versus control, respectively.

Beyond comparing each disease group to the control group, a comparison across tauopathies was conducted (Figure 14). Scaling Log2 peptide intensities for control, AD, FTDP, and PSP samples revealed similar trends within each group, though outliers were identified based on intensity patterns, such as the 8th column in the control group and the first column in the PSP group (Figure 14a). Gene ontology groups significantly enriched in the top cluster included those related to microtubule polymerization, disordered domain-specific binding, and cytoskeletal protein binding—features expected to be increased in controls and decreased in disease due to tau pathology (Figure 14b). In contrast, GO terms enriched in the bottom cluster, such as neuron projection, heat shock protein binding, phosphatase activity, protein serine kinase activity, neuron migration, and chemokine signaling, suggest activation of the cellular stress response. These terms were more intense in disease samples and less intense in controls, highlighting the stress pathways activated in tauopathies (Figure 14c). Additionally, comparison of the overlap in significant phosphopeptides from each group revealed that AD contained more unique phosphopeptides, while FTDP and PSP shared more of their phosphoproteome (Figure 14d).

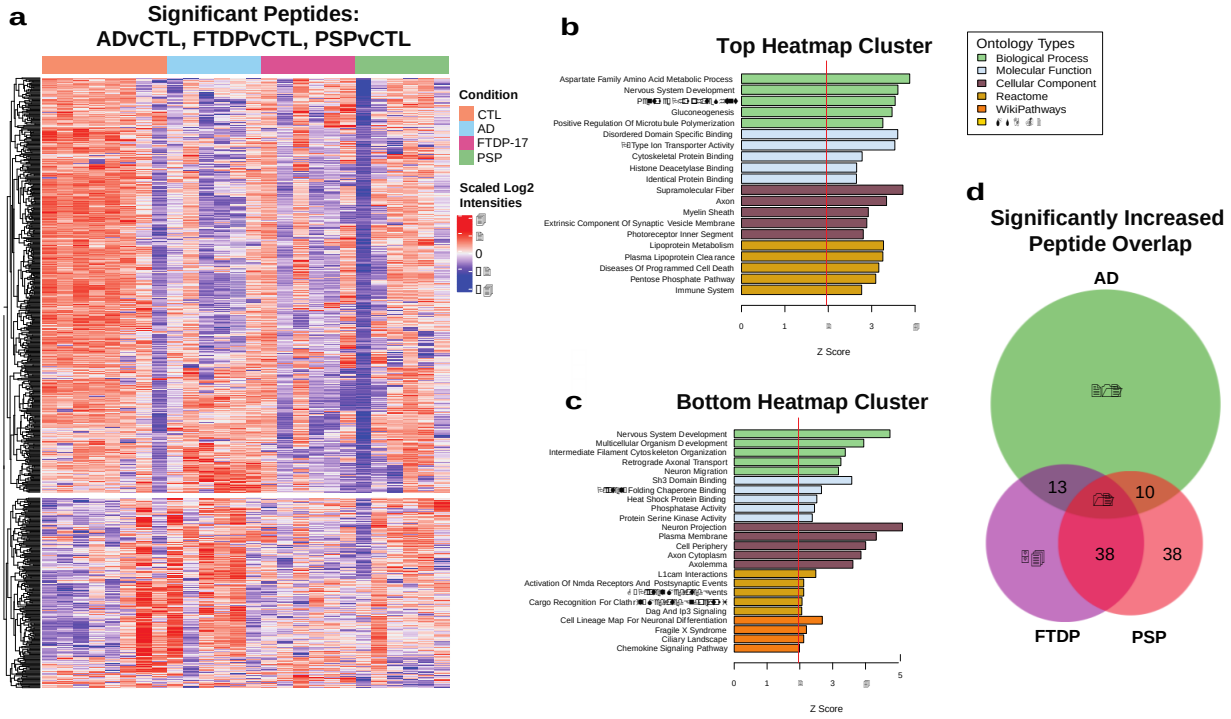


**Figure 14.** Comparison of phosphopeptide enriched proteomes of CTL, AD, FTDP, and CTL.
**a** Heatmap of significant peptides relevant to disease from Figure 4. The log2 fold intensity values across control and tauopathy individual samples were z-scored and scaled for visualization. Greater intensities are colored in hues of red, whereas purple represents lower protein intensities. Sample IDs are colored according to disease group: CTL is orange, AD is blue, FTDP is pink, and PSP is green. Hierarchical clustering analysis was utilized to group protein rows. Significant phosphoproteins determined from one-way ANOVAs plotted on volcano plots from Figure 8 were compared between each tauopathy. **b** Top Gene Ontology (GO) terms for genes present in top cluster from heatmap in a. Fisher Exact Test for enrichment p<0.05 was used to map gene lists onto Biological Process, Molecular Function, Cellular Component, Reactome, WikiPathways, and MSIG.C2 gene lists. **c** Top GO terms for genes present in bottom cluster from heatmap in a. Fisher Exact Test for enrichment p<0.05 was used to map gene lists onto Biological Process, Molecular Function, Cellular Component, Reactome, WikiPathways, and MSIG.C2 gene lists. **d** Phosphopeptides significantly increased in AD, FTDP, and PSP as determined from one-way ANOVAs plotted on volcano plots from Figure 8 were compared to visualize the overlap in their phosphoprotein profiles.

## Chapter 5: Discussion

In this study, immobilized metal affinity chromatography (IMAC) followed by liquid chromatography-tandem mass spectrometry (LC-MS/MS) was used to identify phosphopeptides from tauopathy and control postmortem frontal cortex human brain tissues. The identification of phosphopeptides by mass spectrometry relies upon the mass/charge (m/z) ratios of the detected peptides, where a mass increase of 79.9799 Da represents the phosphorylation PTM.[77] Due to the importance of the experimental masses of the peptides, a mass spectrometer that provides high mass accuracy should be used. Both time-of-flight (TOF) and Orbitrap MS are typically used for phoshoproteomics. In this experiment, the TimsTOF HT was used to enhance proteome coverage and sensitivity. The TimsTOF HT also utilizes a quadrupole mass filter, but it has the added element of Trapped Ion Mobility Spectrometry (TIMS), where ions are separated in the gas phase based on mass and mobility to add an additional layer of separation prior to TOF spectrometry. This added mechanism of separation increases the rate at which complex samples can be analyzed, enabling large cohorts to be quickly analyzed.

The TimsTOF HT can be used with either Data Independent Acquisition (DIA) or Data Dependent Acquisition (DDA) discovery modes. Since DDA selects the most abundant peptides for isolation and fragmentation, the coupling of phosphoenrichment with DDA MS is often used for deep characterization of the phosphoproteome despite its limitations by run-run irreproducibility due to the stochastic selection of abundant peptides.[78] In contrast, DIA isolates peptides within a pre-selected m/z window, which increased reproducibility at the cost of more complex data analysis and fewer unique phosphopeptides identified.[79] For these reasons, DDA MS was utilized for this study.

To overcome the bias of DDA toward selection of highly abundant proteins for MS/MS, the detection of the low abundance peptides must be improved to enhance the depth of the proteome.

Fe-IMAC was used in this study to enrich phosphopeptides, however a successful phosphoenrichment LC-MS/MS workflow requires optimization at several stages. First, phosphate interactions must be preserved throughout the entire workflow. Phosphorylation is a highly dynamic reversible modification. Prior studies conducted in mouse brain demonstrated that proteins were rapidly dephosphorylated to various degrees during 20 seconds to 10 minutes postmortem.[80] Additionally, this dephosphorylation was site specific, with p-tau at Thr205, Ser214, and Ser396 dephosphorylated at a more rapid rate than Ser199, Ser404, and Ser422. Although the brain tissue samples were treated with phosphatase inhibitors, hydrolysis of the phosphate ester bond must be mitigated to achieve the desired depth of the phosphoproteome. To maximize the coverage of the phosphoproteome, phosphate interactions must be preserved throughout the homogenization, digestion, enrichment, and mass spectrometry steps.

To first determine the feasibility of using magnetic Fe-NTA agarose beads to enrich phosphoproteins in brain tissue, several brands of magnetic beads were compared in brain tissue collected from AD and non-demented patients. Ni-NTA magnetic agarose beads from Pierce Thermofisher Scientific and PureCube Cube Biotech were compared in terms of specificity and abundance of phosphopeptide binding end detection. Since the Pierce magnetic agarose beads had a binding capacity of 70mg protein per 1 mL of beads and the PureCube magnetic beads had a binding capacity of 8- mg protein / 1 mL beads, the ratio of beads to protein was normalized to bind 500 μg of protein. Since a greater number of phosphopeptides were captured sing the PureCube beads, these were used for subsequent experiments. The enriched samples identified more than the 3% of phosphopeptides observed in the total proteome before enrichment, indicating the usefulness of this method. However, further optimization is required because prior Fe-IMAC enrichments were able to identify thousands of phosphopeptides, and this method only identified hundreds of peptides across all conditions.[34]

Hyperphosphorylation is a hallmark of AD, and these findings reinforce its role in disease progression. The increase in MAPT (tau) aligns with established literature, emphasizing tau pathology in AD. These enriched isoforms of tau were phosphorylated at various phosphosites, suggesting the importance of site-specific phosphorylation analysis when understanding the progression of pathological changes. Specific kinases are largely responsible for site-specific tau hyperphosphorylation, including members of the Microtubule Affinity Regulating Kinase family (MARK1-4).[73] MAP1B is another microtubule associated protein that works together with tau to crosslink microtubules, supporting axonal extension and neuronal migration.[81] MAP1B has also been shown to be phosphorylated by MARKS, further connecting the aberrant activity of these kinases to defects in cytoskeletal dynamics in AD.[82]

In addition to MARK, Protein kinase C (PKC) frequently phosphorylates microtubule associated proteins. PKC is shown to be involved in amyloid precursor protein (APP) processing with a decrease in PKC activity suggested to correlate with the overproduction of Aβ in AD cortical neurons.[83] PKC phosphorylates myristoylated alanine-rich C kinase substrate (MARCKS), a protein that was significantly enriched in AD in several circumstances in this study. Prior studies show increased MARCKS phosphorylation in Aβ deposits, suggesting a link between PKC activity and the maturation of senile plaques in AD.[83] Furthermore, MARCKS is involved in neuronal migration and neurite outgrowth, similar to tau and MAP1B.[84] The hyperphosphorylation of these proteins observed in this study suggest broader disruptions in microtubule-associated phosphorylation, potentially affecting cytoskeletal stability and neuronal function.

Once the feasibility of using Fe-NTA IMAC beads to enrich phosphoproteins for identification by LC-MS/MS was established, the protocol required further optimization to increase the depth of proteome coverage. Prerequisites of phosphoproteomics include preservation of phosphate

interactions throughout the protein extraction digestion, enrichment and mass spectrometry steps to maximize sampling depth. The impact of several experimental parameters on the success of the phosphoenrichment was recorded: starting protein concentration, Trypsin/Lys-C digestion incubation time, post-digestion drying down, protein-bead binding incubation time, recharging of the beads with FeCl, and elution incubation time.

Previous work performing phosphoenrichment recommend an optimal starting amount of 200- to 500 μg of protein in order to identify low-abundance phosphopeptides[85] However, these numbers were suggested based on *S. cerevisiae* cells. Human samples are more valuable and have a more complex proteome, which may pose a limiting factor. For reference, 1 mg of proteins has been used for isobaric labeling mass spectrometery.[86] This study compared the percent phosphoenrichment by the label-free proteomic workflow compared starting concentrations of 250 μg, 500μg, and 1000μg of protein. The wide variability in proteome coverage and phosphoenrichment in the 250 μg sample suggested that 250 μg of brain tissue may not be sufficient to achieve reproducible results through this protocol. The 500 μg and 1000 μg samples demonstrated similar phosphoproteome coverage, so 500 μg was selected for use in future experiments to conserve sample.

The next step of the workflow is the digestion by trypsin and LysC for phosphopeptide level enrichment. Enrichment can be conducted at the protein and peptide level, with phosphoprotein enrichment being beneficial because it reveals the molecular weight and isoelectric point of proteins. Additionally, mass *spectrometry* identification by protein is more reliable because it is based on several peptides. But protein enrichment sometimes fails to resuspend larger, hydrophobic proteins, extremely alkaline or acidic proteins are difficult to separate, and tiny and hydrophobic proteins are often lost during precipitation steps. Due to the loss of these proteins,

less abundant proteins are not likely to be identified. Additionally, phosphoprotein enrichment is less specific than phosphopeptide enrichment because of the higher complexity structure of proteins. Since phosphoprotein enrichment is beneficial when identifying the most abundance proteins, phosphopeptide enrichment is preferable for phosphoproteomics due to the substoichiometic levels of phosphorylated proteins. However, the removal of non-phosphorylated peptides during the enrichment step means that protein identification relies on one singular peptide, which limits accurate detection. Furthermore, nonspecific binding remains a limiting factor.

However, sample preparation steps prior to mass spectrometry may limit the detection of phosphopeptides. Trypsin, which cleaves peptides at the carboxyterminal of lysine and arginine, and *L*ys-C, which cleaves proteins at the carboxyterminal of lysine, were used for digestion. However, phosphoserine and phosphothreonine may impair protease cleavage.[87] Therefore, increasing the protease concentrations up to 1:20 is beneficial in phosphoproteomic studies to improve digestion efficiency of phosphopeptides resistant to cleavage.[88] Since phosphorylated peptides are more resistant to digestion, limited comparisons between phosphorylated and non-phosphorylated peptides can be accurately made post digestion.[89] To further evaluate the impact of digestion efficiency on phosphoproteomics, the impact of digestion incubation times was tested. Prior studies demonstrated that prolonged incubation times did not improve digestion efficiency beyond 4 hours.[88] Similarly, this study did not observe the digestion incubation time as having a significant impact on proteome coverage, with 1 hour, 4 hour, and overnight incubations showing similar coverage of the phosphoproteome. Considering this, the overnight digestion was utilized for future experiments for convenience.

Since phosphopeptides are represented in low abundances in protein digests, selective phosphoenrichment using Fe-IMAC was used to enhance the relative abundance of

phosphopeptides prior to mass spectrometry. However, to determine if phosphate interactions were being lost when the samples were dried down between the digestion clean up and the phosphoenrichment steps, one sample was stored in binding buffer overnight prior to enrichment instead of being dried down. These samples, where the drying down was skipped, showed similar phosphoproteomic coverage than the samples that were dried down, so it did not appear that phosphate groups are lost in high quantities by drying the samples down.

To further optimize the enrichment step, the impact of incubation time of the brain tissue lysates with the Fe-NTA agarose beads on binding specifically was observed by comparing a 30 minute and a 2-hour incubation. Fewer total proteins were detected from the samples with a 2-hour binding incubation time, but the percentage of phosphopeptides was high in both samples, indicting a longer incubation time may promote binding specificity. While enrichment conducted at an acidic pH deprotonates the phosphate groups to facilitate their binding to Fe, the extended incubation likely also further enabled the phosphopeptides to better outcompete non-phosphorylated peptides for Fe-NTA binding sites. However, prolonged incubation may also introduce potential drawbacks, such as weakened ionic interactions over time and fewer bound peptides. Despite the higher specificity, a 30-minute binding time was used for future experiments to improve total phosphopeptide binding.

The preliminary experiment conducted in this study involved Ni-NTA magnetic beads that were stripped with EDTA and recharged with Fe-CL. Additionally, the agarose beads (both Fe-NTA and Ni-NTA beads) sold by Cube Biotech can be stripped, recharged, and reused. To observe the efficiency of the recharging of the beads, Ni-NTA beads were stripped and recharged and compared to fresh Fe-NTA magnetic beads. While there was variability in the beads Fe-NTA phosphoenrichment capabilities, there was not a clear difference between the recharged beads

and the brand-new beads, confirming that the stripping and recharging of the beads does not impact the success of the workflow.

The final parameter to be evaluated was the elution step. Previous studies have optimized the elution buffer for this experiment, but there was variability in the literature regarding incubation time in the elution buffer prior to collection of the phosphoproteome.[70,85] A 30 minute elution incubation appeared to elute non-phosphorylated proteins from the Fe-NTA beads without eluting more phosphopeptides than the 1 minute elution incubation time. This led to the identification of fewer phosphopeptides, prompting a 1-minute incubation to be used for future studies.

Overall, this study established a phosphoenrichment LC-MS/MS workflow that effectively captures phosphorylated peptides from human AD brain tissue. While significant progress was made in optimizing the method, additional refinements may be necessary to improve phosphoproteome depth further. Future work will focus on integrating complementary enrichment strategies and leveraging advanced bioinformatics tools to enhance phosphopeptide identification and biological interpretation. These efforts will contribute to a more comprehensive understanding of phosphorylation-driven mechanisms in AD pathogenesis and may inform potential therapeutic targets.

After optimizing the phosphoenrichment pipeline, its application to larger cohorts of samples needed to be validated. AD, FTDP, and PSP are all tauopathies, grouped due to their shared tau pathology, resulting in neuronal loss and brain atrophy. Clinical symptoms often involve cognitive decline, behavioral changes, and movement impairments, causing differentiation between these conditions to be difficult due to their overlapping symptoms. Comparing the phosphoprotein profiles of AD, FTDP, and PSP may provide insight into the proteins both distinct to these diseases and conserved across the tauopathy pathological state. Gaining a deeper understanding of the molecular signatures of AD, FTDP, and PSP will help clarify the pathological differences between

these diseases, which share tau-related pathology involving neurofibrillary tangles made of paired helical filaments composed of abnormally phosphorylated tau.[90] So, identifying the factors responsible for tau hyperphosphorylation may uncover commonalities across these conditions, highlighting the significance of investigating kinase and phosphatase profiles in each unique disease state.

Prior studies have demonstrated that increased levels of hyperphosphorylated tau are commonly found in tauopathies, though this pattern can be disease specific. In frontotemporal dementia with Parkinsonism (FTDP), hyperphosphorylated tau is present, along with abundant filamentous tau pathology. However, hyperphosphorylation is not considered a critical component of the filamentous tau pathology in FTDP. Instead, a shift in the ratio of 3-repeat (3R) to 4-repeat (4R) tau isoforms is sufficient to drive the development of filamentous tau pathology.[91,92] Similarly, the tau pathology seen in progressive supranuclear palsy (PSP) resembles that of FTDP, with filamentous tau deposits present in both neuronal and glial cells. [3]

However, despite their shared tau pathology, prior studies have reported differences in the phosphoprotein profiles of tauopathies.[93] AD, FTDP, and PSP show different levels of phosphorylated tau. For example, Thr205, and Ser235 were shown to be phosphorylated more in AD than other tauopathies. However, some phosphosites are significantly phosphorylated in control samples, such as Ser404. Additionally, the same study also reported variation between patient samples of the same tauopathy, as seen in Figure 10. Accordingly, PSP was shown to have 2 distinct phosphorylation patterns, perhaps explaining the variation observed throughout this project.

As expected, more MAPT isoforms were phosphorylated in AD than FTDP and PSP when compared to controls. However, it was surprising that MAPT was observed as decreased in FTDP

especially. Especially considering MAPT p-Tyr217 was decreased in FTDP and MAPT p-Tyr231 was decreased in PSP, both of which are considered early biomarkers of AD pathology and commonly phosphorylated in tauopathies. Significant MAPT phosphosites will be validated via western blot to support the claims derived from the mass spectrometry results. But the western blots from Figure 11 do show similar levels of p-tau 396 in CTL, FTDP, and PSP samples, perhaps explaining the unexpected tau results. EPB41L3, a protein that enables cytoskeletal protein-membrane anchor activity, is decreased in AD, FTDP, and PSP/ his aligns with the microtubule dissociation and breakdown in cytoskeletal organization associated with tau hyperphosphorylation. Accordingly GO terms involving cytoskeletal organization are decreased across the tauopathies, prompting further investigation into the impact of phosphorylation on cytoskeleton structure in the disease state.

The heatmap from Figure 14a clearly shows a divide between the protein intensity pattern observed in control samples versus the tauopathy samples, with further division occurring between each tauopathy. Better understanding the shared gene ontology groups across the tauopathy disease states may lead to a deeper understanding of the role of the phosphoproteins in the diseased state. For example, the response to unfolder protein response and chaperone mediated autophagy are increased in AD, which aligns with the cell's response to tau protein aggregates. However, the increase in protein phosphatase binding is surprising because increased phosphatase activity should lead to reduced phosphorylation. Further investigation into the fluctuations of phosphatase activity over the gene timeline will be useful for characterizing the changes to the AD proteome over the course of the disease.

The neuromuscular process GO term is increased in FTDP, aligning with the predominant muscular stiffness seen in the disease. Better understanding these proteins may assist in differentiating FTDP from AD and PSP at the neuropathological level. Since FTDP and PSP had

more similar phosphoprotein profiles than with AD, future studies should further investigate their phosphoproteins in search of unique biomarkers. This would be useful if applied to biofluid studies since FTDP and PSP are largely diagnosed neuropathologically postmortem.

Building on this study, future applications of this method will involve optimizing for high throughput enrichment of phosphopeptides. Benefits of developing this phosphoenrichment procedure are that the magnetic agarose beads are compatible with the Kingfisher Apex, a machine capable of robotically performing the enrichment workflow in a 96 well plate.[94] This will facilitate phosphoproteomic studies of large cohorts in order to strengthen our understanding of the role of phosphorylation in disease to determine proteins with clinical significance for diagnostic and treatment.

However, limitations of this method involve the preservation of phosphate interactions, which often deteriorate rapidly post harvesting of the brains and throughout sample processing. Additionally, the phosphate group may impair enzymatic cleavage, causing knowledge about some phosphate sites to be lost. Additionally, non-specific binding to the agarose beads during phosphopeptide enrichment hinders the signal of some phosphopeptides, which may require further optimization as this method is scaled up. Also, secondary enrichment may be required using $TiO_2$ or $ZrO_2$ to capture proteins that do not have a strong affinity for iron to increase the depth of the proteome. Significant variability was observed in the proteome coverage of this study, which may be overcome though the use of a robotic high throughput affinity purification instrument. Furthermore, protein identification relies on one peptide and DDA favors abundant peptides, suggesting that DIA mass spectrometry may enhance the reproducibility of this method. Finally, cell specific information is lost when using this pipeline on whole brain tissue lysates, so single cell experiments would be interesting to observe the role of phosphorylation within neurons, glia, and other cells in the brain.

Knowing that current studies are emphasizing our understanding of AD biomarkers in CSF and plasma to develop more accurate and accessible diagnostics, it would be beneficial to adapt this protocol to biofluids. However, the large amount of protein required for this protocol limits the use of biofluids, so further optimization is required due to the differences in phosphopeptide concentration in brain, CSF, and plasma. Expanding this approach to biofluids could standardize phosphoproteomics across neurodegeneration research, strengthening the depth of our knowledge of the phosphoproteins implicated in these diseases and exposing new opportunities to develop therapeutics and diagnostic targets.

**References**


(1) Rawat, P.; Sehar, U.; Bisht, J.; Selman, A.; Culberson, J.; Reddy, P. H. Phosphorylated Tau in Alzheimer's Disease and Other Tauopathies. *Int J Mol Sci* **2022**, *23* (21), 12841. https://doi.org/10.3390/ijms232112841.

(2) Nishi, H.; Hashimoto, K.; Panchenko, A. R. Phosphorylation in Protein-Protein Binding: Effect on Stability and Function. *Structure* **2011**, *19* (12), 1807–1815. https://doi.org/10.1016/j.str.2011.09.021.

(3) Cohen, P. The Role of Protein Phosphorylation in Human Health and Disease. *European Journal of Biochemistry* **2001**, *268* (19), 5001–5010. https://doi.org/10.1046/j.0014-2956.2001.02473.x.

(4) Johnson, L. N.; Lewis, R. J. Structural Basis for Control by Phosphorylation. *Chem. Rev.* **2001**, *101* (8), 2209–2242. https://doi.org/10.1021/cr000225s.

(5) Li, X.; Wilmanns, M.; Thornton, J.; Köhn, M. Elucidating Human Phosphatase-Substrate Networks. *Science Signaling* **2013**, *6* (275), rs10–rs10. https://doi.org/10.1126/scisignal.2003203.

(6) Manning, G.; Whyte, D. B.; Martinez, R.; Hunter, T.; Sudarsanam, S. The Protein Kinase Complement of the Human Genome. *Science* **2002**, *298* (5600), 1912–1934. https://doi.org/10.1126/science.1075762.

(7) Chen, M. J.; Dixon, J. E.; Manning, G. Genomics and Evolution of Protein Phosphatases. *Science Signaling* **2017**, *10* (474), eaag1796. https://doi.org/10.1126/scisignal.aag1796.

(8) Stern, D. F. Phosphoproteomics for Oncology Discovery and Treatment. *Expert Opin Ther Targets* **2005**, *9* (4), 851–860. https://doi.org/10.1517/14728222.9.4.851.

(9) Radivojac, P.; Baenziger, P. H.; Kann, M. G.; Mort, M. E.; Hahn, M. W.; Mooney, S. D. Gain and Loss of Phosphorylation Sites in Human Cancer. *Bioinformatics* **2008**, *24* (16), i241–i247. https://doi.org/10.1093/bioinformatics/btn267.

(10) Kreisberg, J. I.; Malik, S. N.; Prihoda, T. J.; Bedolla, R. G.; Troyer, D. A.; Kreisberg, S.; Ghosh, P. M. Phosphorylation of Akt (Ser473) Is an Excellent Predictor of Poor Clinical Outcome in Prostate Cancer. *Cancer Research* **2004**, *64* (15), 5232–5236. https://doi.org/10.1158/0008-5472.CAN-04-0272.

(11) Lee, M. Y.; Joung, Y. H.; Lim, E. J.; Park, J.-H.; Ye, S.-K.; Park, T.; Zhang, Z.; Park, D. K.; Lee, K. J.; Yang, Y. M. Phosphorylation and Activation of STAT Proteins by Hypoxia in Breast Cancer Cells. *The Breast* **2006**, *15* (2), 187–195. https://doi.org/10.1016/j.breast.2005.05.005.

(12) Farrell, A. S.; Allen-Petersen, B.; Daniel, C. J.; Wang, X.; Wang, Z.; Rodriguez, S.; Impey, S.; Oddo, J.; Vitek, M. P.; Lopez, C.; Christensen, D. J.; Sheppard, B.; Sears, R. C. Targeting Inhibitors of the Tumor Suppressor PP2A for the Treatment of Pancreatic Cancer. *Molecular Cancer Research* **2014**, *12* (6), 924–939. https://doi.org/10.1158/1541-7786.MCR-13-0542.

(13) Tenreiro, S.; Eckermann, K.; Outeiro, T. F. Protein Phosphorylation in Neurodegeneration: Friend or Foe? *Front. Mol. Neurosci.* **2014**, *7*. https://doi.org/10.3389/fnmol.2014.00042.

(14) Zhou, J.; Broe, M.; Huang, Y.; Anderson, J. P.; Gai, W.-P.; Milward, E. A.; Porritt, M.; Howells, D.; Hughes, A. J.; Wang, X.; Halliday, G. M. Changes in the Solubility and Phosphorylation of α-Synuclein over the Course of Parkinson's Disease. *Acta Neuropathol* **2011**, *121* (6), 695–704. https://doi.org/10.1007/s00401-011-0815-1.

(15) Colom-Cadena, M.; Pegueroles, J.; Herrmann, A. G.; Henstridge, C. M.; Muñoz, L.; Querol-Vilaseca, M.; Martín-Paniello, C. S.; Luque-Cabecerans, J.; Clarimon, J.; Belbin, O.; Núñez-Llaves, R.; Blesa, R.; Smith, C.; McKenzie, C.-A.; Frosch, M. P.; Roe, A.; Fortea, J.; Andilla, J.; Loza-Alvarez, P.; Gelpi, E.; Hyman, B. T.; Spires-Jones, T. L.; Lleó, A. Synaptic Phosphorylated α-Synuclein in Dementia with Lewy Bodies. *Brain* **2017**, *140* (12), 3204–3214. https://doi.org/10.1093/brain/awx275.

(16) Coughlin, D.; Xie, S. X.; Liang, M.; Williams, A.; Peterson, C.; Weintraub, D.; McMillan, C. T.; Wolk, D. A.; Akhtar, R. S.; Hurtig, H. I.; Branch Coslett, H.; Hamilton, R. H.; Siderowf, A. D.; Duda, J. E.; Rascovsky, K.; Lee, E. B.; Lee, V. M.-Y.; Grossman, M.; Trojanowski, J. Q.; Irwin, D. J. Cognitive and Pathological Influences of Tau Pathology in Lewy Body Disorders. *Annals of Neurology* **2019**, *85* (2), 259–271. https://doi.org/10.1002/ana.25392.

(17) Drechsel, D. N.; Hyman, A. A.; Cobb, M. H.; Kirschner, M. W. Modulation of the Dynamic Instability of Tubulin Assembly by the Microtubule-Associated Protein Tau. *Mol Biol Cell* **1992**, *3* (10), 1141–1154.

(18) Kadavath, H.; Hofele, R. V.; Biernat, J.; Kumar, S.; Tepper, K.; Urlaub, H.; Mandelkow, E.; Zweckstetter, M. Tau Stabilizes Microtubules by Binding at the Interface between Tubulin Heterodimers. *Proc Natl Acad Sci U S A* **2015**, *112* (24), 7501–7506. https://doi.org/10.1073/pnas.1504081112.

(19) Daebel, V.; Chinnathambi, S.; Biernat, J.; Schwalbe, M.; Habenstein, B.; Loquet, A.; Akoury, E.; Tepper, K.; Müller, H.; Baldus, M.; Griesinger, C.; Zweckstetter, M.; Mandelkow, E.; Vijayan, V.; Lange, A. β-Sheet Core of Tau Paired Helical Filaments Revealed by Solid-State NMR. *J Am Chem Soc* **2012**, *134* (34), 13982–13989. https://doi.org/10.1021/ja305470p.

(20) Hill, E.; Karikari, T. K.; Lantero-Rodriguez, J.; Zetterberg, H.; Blennow, K.; Richardson, M. J.; Wall, M. J. Truncating Tau Reveals Different Pathophysiological Actions of Oligomers in Single Neurons. *Commun Biol* **2021**, *4* (1). https://doi.org/10.1038/s42003-021-02791-x.

(21) Strang, K. H.; Golde, T. E.; Giasson, B. I. *MAPT* Mutations, Tauopathy, and Mechanisms of Neurodegeneration. *Laboratory Investigation* **2019**, *99* (7), 912–928. https://doi.org/10.1038/s41374-019-0197-x.

(22) Hutton, M.; Lendon, C. L.; Rizzu, P.; Baker, M.; Froelich, S.; Houlden, H.; Pickering-Brown, S.; Chakraverty, S.; Isaacs, A.; Grover, A.; Hackett, J.; Adamson, J.; Lincoln, S.; Dickson, D.; Davies, P.; Petersen, R. C.; Stevens, M.; de Graaff, E.; Wauters, E.; van Baren, J.; Hillebrand, M.; Joosse, M.; Kwon, J. M.; Nowotny, P.; Che, L. K.;

Norton, J.; Morris, J. C.; Reed, L. A.; Trojanowski, J.; Basun, H.; Lannfelt, L.; Neystat, M.; Fahn, S.; Dark, F.; Tannenberg, T.; Dodd, P. R.; Hayward, N.; Kwok, J. B.; Schofield, P. R.; Andreadis, A.; Snowden, J.; Craufurd, D.; Neary, D.; Owen, F.; Oostra, B. A.; Hardy, J.; Goate, A.; van Swieten, J.; Mann, D.; Lynch, T.; Heutink, P. Association of Missense and 5'-Splice-Site Mutations in Tau with the Inherited Dementia FTDP-17. *Nature* **1998**, *393* (6686), 702–705. https://doi.org/10.1038/31508.

(23) Zhang, Y.; Wu, K.-M.; Yang, L.; Dong, Q.; Yu, J.-T. Tauopathies: New Perspectives and Challenges. *Molecular Neurodegeneration* **2022**, *17* (1), 28. https://doi.org/10.1186/s13024-022-00533-z.

(24) Crary, J. F.; Trojanowski, J. Q.; Schneider, J. A.; Abisambra, J. F.; Abner, E. L.; Alafuzoff, I.; Arnold, S. E.; Attems, J.; Beach, T. G.; Bigio, E. H.; Cairns, N. J.; Dickson, D. W.; Gearing, M.; Grinberg, L. T.; Hof, P. R.; Hyman, B. T.; Jellinger, K.; Jicha, G. A.; Kovacs, G. G.; Knopman, D. S.; Kofler, J.; Kukull, W. A.; Mackenzie, I. R.; Masliah, E.; McKee, A.; Montine, T. J.; Murray, M. E.; Neltner, J. H.; Santa-Maria, I.; Seeley, W. W.; Serrano-Pozo, A.; Shelanski, M. L.; Stein, T.; Takao, M.; Thal, D. R.; Toledo, J. B.; Troncoso, J. C.; Vonsattel, J. P.; White, C. L.; Wisniewski, T.; Woltjer, R. L.; Yamada, M.; Nelson, P. T. Primary Age-Related Tauopathy (PART): A Common Pathology Associated with Human Aging. *Acta Neuropathol* **2014**, *128* (6), 755–766. https://doi.org/10.1007/s00401-014-1349-0.

(25) Crary, J. F. Primary Age-Related Tauopathy and the Amyloid Cascade Hypothesis: The Exception That Proves the Rule? *Journal of Neurology & Neuromedicine* **2016**, *1* (6).

(26) Iida, M. A.; Farrell, K.; Walker, J. M.; Richardson, T. E.; Marx, G. A.; Bryce, C. H.; Purohit, D.; Ayalon, G.; Beach, T. G.; Bigio, E. H.; Cortes, E. P.; Gearing, M.; Haroutunian, V.; McMillan, C. T.; Lee, E. B.; Dickson, D. W.; McKee, A. C.; Stein, T. D.; Trojanowski, J. Q.; Woltjer, R. L.; Kovacs, G. G.; Kofler, J. K.; Kaye, J.; White, C. L.; Crary, J. F. Predictors of Cognitive Impairment in Primary Age-Related Tauopathy: An Autopsy Study. *Acta Neuropathologica Communications* **2021**, *9* (1), 134. https://doi.org/10.1186/s40478-021-01233-3.

(27) Saha, P.; Sen, N. Tauopathy: A Common Mechanism for Neurodegeneration and Brain Aging. *Mechanisms of Ageing and Development* **2019**, *178*, 72–79. https://doi.org/10.1016/j.mad.2019.01.007.

(28) Hippius, H.; Neundörfer, G. The Discovery of Alzheimer's Disease. *Dialogues Clin Neurosci* **2003**, *5* (1), 101–108.

(29) Li, X.; Feng, X.; Sun, X.; Hou, N.; Han, F.; Liu, Y. Global, Regional, and National Burden of Alzheimer's Disease and Other Dementias, 1990–2019. *Front. Aging Neurosci.* **2022**, *14*. https://doi.org/10.3389/fnagi.2022.937486.

(30) McKhann, G.; Drachman, D.; Folstein, M.; Katzman, R.; Price, D.; Stadlan, E. M. Clinical Diagnosis of Alzheimer's Disease: Report of the NINCDS-ADRDA Work Group under the Auspices of Department of Health and Human Services Task Force on Alzheimer's Disease. *Neurology* **1984**, *34* (7), 939–944. https://doi.org/10.1212/wnl.34.7.939.

(31) Yaari, R.; Fleisher, A. S.; Tariot, P. N. Updates to Diagnostic Guidelines for Alzheimer's Disease. *Prim Care Companion CNS Disord* **2011**, *13* (5), PCC.11f01262. https://doi.org/10.4088/PCC.11f01262.

(32) Roda, A. R.; Serra-Mir, G.; Montoliu-Gaya, L.; Tiessler, L.; Villegas, S. Amyloid-Beta Peptide and Tau Protein Crosstalk in Alzheimer's Disease. *Neural Regeneration Research* **2022**, *17* (8), 1666. https://doi.org/10.4103/1673-5374.332127.

(33) Bennett, D. A.; Schneider, J. A.; Wilson, R. S.; Bienias, J. L.; Arnold, S. E. Neurofibrillary Tangles Mediate the Association of Amyloid Load With Clinical Alzheimer Disease and Level of Cognitive Function. *Archives of Neurology* **2004**, *61* (3), 378–384. https://doi.org/10.1001/archneur.61.3.378.

(34) Ping, L.; Kundinger, S. R.; Duong, D. M.; Yin, L.; Gearing, M.; Lah, J. J.; Levey, A. I.; Seyfried, N. T. Global Quantitative Analysis of the Human Brain Proteome and Phosphoproteome in Alzheimer's Disease. *Sci Data* **2020**, *7* (1), 315. https://doi.org/10.1038/s41597-020-00650-8.

(35) Jack Jr., C. R.; Andrews, J. S.; Beach, T. G.; Buracchio, T.; Dunn, B.; Graf, A.; Hansson, O.; Ho, C.; Jagust, W.; McDade, E.; Molinuevo, J. L.; Okonkwo, O. C.; Pani, L.; Rafii, M. S.; Scheltens, P.; Siemers, E.; Snyder, H. M.; Sperling, R.; Teunissen, C. E.; Carrillo, M. C. Revised Criteria for Diagnosis and Staging of Alzheimer's Disease: Alzheimer's Association Workgroup. *Alzheimer's & Dementia* **2024**, *20* (8), 5143–5169. https://doi.org/10.1002/alz.13859.

(36) Spatt, J. Arnold Pick's Concept of Dementia. *Cortex* **2003**, *39* (3), 525–531. https://doi.org/10.1016/S0010-9452(08)70262-4.

(37) Coyle-Gilchrist, I. T. S.; Dick, K. M.; Patterson, K.; Vázquez Rodríquez, P.; Wehmann, E.; Wilcox, A.; Lansdall, C. J.; Dawson, K. E.; Wiggins, J.; Mead, S.; Brayne, C.; Rowe, J. B. Prevalence, Characteristics, and Survival of Frontotemporal Lobar Degeneration Syndromes. *Neurology* **2016**, *86* (18), 1736–1743. https://doi.org/10.1212/WNL.0000000000002638.

(38) Foster, N. L.; Wilhelmsen, K.; Sima, A. A. F.; Jones, M. Z.; D'Amato, C. J.; Gilman, S.; Participants, C. Frontotemporal Dementia and Parkinsonism Linked to Chromosome 17: A Consensus Conference. *Annals of Neurology* **1997**, *41* (6), 706–715. https://doi.org/10.1002/ana.410410606.

(39) Wszolek, Z. K.; Tsuboi, Y.; Ghetti, B.; Pickering-Brown, S.; Baba, Y.; Cheshire, W. P. Frontotemporal Dementia and Parkinsonism Linked to Chromosome 17 (FTDP-17). *Orphanet J Rare Dis* **2006**, *1*, 30. https://doi.org/10.1186/1750-1172-1-30.

(40) Stanford, P. M.; Shepherd, C. E.; Halliday, G. M.; Brooks, W. S.; Schofield, P. W.; Brodaty, H.; Martins, R. N.; Kwok, J. B. J.; Schofield, P. R. Mutations in the Tau Gene That Cause an Increase in Three Repeat Tau and Frontotemporal Dementia. *Brain* **2003**, *126* (4), 814–826. https://doi.org/10.1093/brain/awg090.
(41) Spillantini, M. G.; Bird, T. D.; Ghetti, B. Frontotemporal Dementia and Parkinsonism Linked to Chromosome 17: A New Group of Tauopathies. *Brain Pathology* **1998**, *8* (2), 387–402. https://doi.org/10.1111/j.1750-3639.1998.tb00162.x.
(42) Goedert, M.; Spillantini, M. G. Tau Mutations in Frontotemporal Dementia FTDP-17 and Their Relevance for Alzheimer's Disease. *Biochimica et Biophysica Acta (BBA) - Molecular Basis of Disease* **2000**, *1502* (1), 110–121. https://doi.org/10.1016/S0925-4439(00)00037-5.
(43) STEELE, J. C.; RICHARDSON, J. C.; OLSZEWSKI, J. Progressive Supranuclear Palsy: A Heterogeneous Degeneration Involving the Brain Stem, Basal Ganglia and Cerebellum With Vertical Gaze and Pseudobulbar Palsy, Nuchal Dystonia and Dementia. *Archives of Neurology* **1964**, *10* (4), 333–359. https://doi.org/10.1001/archneur.1964.00460160003001.
(44) Boxer, A. L.; Yu, J.-T.; Golbe, L. I.; Litvan, I.; Lang, A. E.; Höglinger, G. U. Advances in Progressive Supranuclear Palsy: New Diagnostic Criteria, Biomarkers, and Therapeutic Approaches. *The Lancet Neurology* **2017**, *16* (7), 552–563. https://doi.org/10.1016/S1474-4422(17)30157-6.
(45) Briggs, M.; Allinson, K. S.; Malpetti, M.; Spillantini, M. G.; Rowe, J. B.; Kaalund, S. S. Validation of the New Pathology Staging System for Progressive Supranuclear Palsy. medRxiv January 25, 2021, p 2021.01.18.21250017. https://doi.org/10.1101/2021.01.18.21250017.
(46) Höglinger, G. U.; Respondek, G.; Stamelou, M.; Kurz, C.; Josephs, K. A.; Lang, A. E.; Mollenhauer, B.; Müller, U.; Nilsson, C.; Whitwell, J. L.; Arzberger, T.; Englund, E.; Gelpi, E.; Giese, A.; Irwin, D. J.; Meissner, W. G.; Pantelyat, A.; Rajput, A.; van Swieten, J. C.; Troakes, C.; Antonini, A.; Bhatia, K. P.; Bordelon, Y.; Compta, Y.; Corvol, J.-C.; Colosimo, C.; Dickson, D. W.; Dodel, R.; Ferguson, L.; Grossman, M.; Kassubek, J.; Krismer, F.; Levin, J.; Lorenzl, S.; Morris, H. R.; Nestor, P.; Oertel, W. H.; Poewe, W.; Rabinovici, G.; Rowe, J. B.; Schellenberg, G. D.; Seppi, K.; van Eimeren, T.; Wenning, G. K.; Boxer, A. L.; Golbe, L. I.; Litvan, I.; Movement Disorder Society-endorsed PSP Study Group. Clinical Diagnosis of Progressive Supranuclear Palsy: The Movement Disorder Society Criteria. *Mov Disord* **2017**, *32* (6), 853–864. https://doi.org/10.1002/mds.26987.
(47) Laske, C.; Sohrabi, H. R.; Frost, S. M.; López-de-Ipiña, K.; Garrard, P.; Buscema, M.; Dauwels, J.; Soekadar, S. R.; Mueller, S.; Linnemann, C.; Bridenbaugh, S. A.; Kanagasingam, Y.; Martins, R. N.; O'Bryant, S. E. Innovative Diagnostic Tools for Early Detection of Alzheimer's Disease. *Alzheimer's & Dementia* **2015**, *11* (5), 561–578. https://doi.org/10.1016/j.jalz.2014.06.004.
(48) Wongso, H.; Harada, R.; Furumoto, S. Current Progress and Future Directions in Non-Alzheimer's Disease Tau PET Tracers. *ACS Chem. Neurosci.* **2025**, *16* (2), 111–127. https://doi.org/10.1021/acschemneuro.4c00319.
(49) Fleisher, A. S.; Pontecorvo, M. J.; Devous, M. D., Sr; Lu, M.; Arora, A. K.; Truocchio, S. P.; Aldea, P.; Flitter, M.; Locascio, T.; Devine, M.; Siderowf, A.; Beach, T. G.; Montine, T. J.; Serrano, G. E.; Curtis, C.; Perrin, A.; Salloway, S.; Daniel, M.; Wellman, C.; Joshi, A. D.; Irwin, D. J.; Lowe, V. J.; Seeley, W. W.; Ikonomovic, M. D.; Masdeu, J. C.; Kennedy, I.; Harris, T.; Navitsky, M.; Southekal, S.; Mintun, M. A.; A16 Study Investigators. Positron Emission Tomography Imaging With [18F]Flortaucipir and Postmortem Assessment of Alzheimer Disease Neuropathologic Changes. *JAMA Neurology* **2020**, *77* (7), 829–839. https://doi.org/10.1001/jamaneurol.2020.0528.
(50) Ossenkoppele, R.; Rabinovici, G. D.; Smith, R.; Cho, H.; Schöll, M.; Strandberg, O.; Palmqvist, S.; Mattsson, N.; Janelidze, S.; Santillo, A.; Ohlsson, T.; Jögi, J.; Tsai, R.; La Joie, R.; Kramer, J.; Boxer, A. L.; Gorno-Tempini, M. L.; Miller, B. L.; Choi, J. Y.; Ryu, Y. H.; Lyoo, C. H.; Hansson, O. Discriminative Accuracy of [18F]Flortaucipir Positron Emission Tomography for Alzheimer Disease vs Other Neurodegenerative Disorders. *JAMA* **2018**, *320* (11), 1151–1162. https://doi.org/10.1001/jama.2018.12917.
(51) Salvadó, G.; Horie, K.; Barthélemy, N. R.; Vogel, J. W.; Pichet Binette, A.; Chen, C. D.; Aschenbrenner, A. J.; Gordon, B. A.; Benzinger, T. L. S.; Holtzman, D. M.; Morris, J. C.; Palmqvist, S.; Stomrud, E.; Janelidze, S.; Ossenkoppele, R.; Schindler, S. E.; Bateman, R. J.; Hansson, O. Disease Staging of Alzheimer's Disease Using a CSF-Based Biomarker Model. *Nat Aging* **2024**, *4* (5), 694–708. https://doi.org/10.1038/s43587-024-00599-y.
(52) Blennow, K.; Chen, C.; Cicognola, C.; Wildsmith, K. R.; Manser, P. T.; Bohorquez, S. M. S.; Zhang, Z.; Xie, B.; Peng, J.; Hansson, O.; Kvartsberg, H.; Portelius, E.; Zetterberg, H.; Lashley, T.; Brinkmalm, G.; Kerchner, G. A.; Weimer, R. M.; Ye, K.; Höglund, K. Cerebrospinal Fluid Tau Fragment Correlates with Tau PET: A Candidate Biomarker for Tangle Pathology. *Brain* **2020**, *143* (2), 650–660. https://doi.org/10.1093/brain/awz346.
(53) Barthélemy, N. R.; Saef, B.; Li, Y.; Gordon, B. A.; He, Y.; Horie, K.; Stomrud, E.; Salvadó, G.; Janelidze, S.; Sato, C.; Ovod, V.; Henson, R. L.; Fagan, A. M.; Benzinger, T. L. S.; Xiong, C.; Morris, J. C.; Hansson, O.; Bateman, R. J.; Schindler, S. E. CSF Tau Phosphorylation Occupancies at T217 and T205 Represent Improved Biomarkers of Amyloid and Tau Pathology in Alzheimer's Disease. *Nat Aging* **2023**, *3* (4), 391–401. https://doi.org/10.1038/s43587-023-00380-7.
(54) Ashton, N. J.; Benedet, A. L.; Pascoal, T. A.; Karikari, T. K.; Lantero-Rodriguez, J.; Brum, W. S.; Mathotaarachchi, S.; Therriault, J.; Savard, M.; Chamoun, M.; Stoops, E.; Francois, C.; Vanmechelen, E.; Gauthier, S.; Zimmer, E. R.; Zetterberg, H.; Blennow, K.; Rosa-Neto, P. Cerebrospinal Fluid P-Tau231 as an

Early Indicator of Emerging Pathology in Alzheimer's Disease. *EBioMedicine* **2022**, *76*. https://doi.org/10.1016/j.ebiom.2022.103836.
(55) Tropea, T. F.; Waligorska, T.; Xie, S. X.; Nasrallah, I. M.; Cousins, K. A. Q.; Trojanowski, J. Q.; Grossman, M.; Irwin, D. J.; Weintraub, D.; Lee, E. B.; Wolk, D. A.; Chen-Plotkin, A. S.; Shaw, L. M.; Initiative, the A. D. N. Plasma Phosphorylated Tau181 Predicts Cognitive and Functional Decline. *Annals of Clinical and Translational Neurology* **2022**, *10* (1), 18. https://doi.org/10.1002/acn3.51695.
(56) Cummings, J.; Aisen, P.; Lemere, C.; Atri, A.; Sabbagh, M.; Salloway, S. Aducanumab Produced a Clinically Meaningful Benefit in Association with Amyloid Lowering. *Alzheimer's Research & Therapy* **2021**, *13* (1), 98. https://doi.org/10.1186/s13195-021-00838-z.
(57) van Dyck, C. H.; Swanson, C. J.; Aisen, P.; Bateman, R. J.; Chen, C.; Gee, M.; Kanekiyo, M.; Li, D.; Reyderman, L.; Cohen, S.; Froelich, L.; Katayama, S.; Sabbagh, M.; Vellas, B.; Watson, D.; Dhadda, S.; Irizarry, M.; Kramer, L. D.; Iwatsubo, T. Lecanemab in Early Alzheimer's Disease. *N Engl J Med* **2023**, *388* (1), 9–21. https://doi.org/10.1056/NEJMoa2212948.
(58) Hartz, R. A.; Ahuja, V. T.; Sivaprakasam, P.; Xiao, H.; Krause, C. M.; Clarke, W. J.; Kish, K.; Lewis, H.; Szapiel, N.; Ravirala, R.; Mutalik, S.; Nakmode, D.; Shah, D.; Burton, C. R.; Macor, J. E.; Dubowchik, G. M. Design, Structure–Activity Relationships, and In Vivo Evaluation of Potent and Brain-Penetrant Imidazo[1,2-b]Pyridazines as Glycogen Synthase Kinase-3β (GSK-3β) Inhibitors. *J. Med. Chem.* **2023**, *66* (6), 4231–4252. https://doi.org/10.1021/acs.jmedchem.3c00133.
(59) Zheng, Y.-L.; Kesavapany, S.; Gravell, M.; Hamilton, R. S.; Schubert, M.; Amin, N.; Albers, W.; Grant, P.; Pant, H. C. A Cdk5 Inhibitory Peptide Reduces Tau Hyperphosphorylation and Apoptosis in Neurons. *EMBO J* **2005**, *24* (1), 209–220. https://doi.org/10.1038/sj.emboj.7600441.
(60) Lv, J.; Shen, X.; Shen, X.; Zhao, S.; Xu, R.; Yan, Q.; Lu, J.; Zhu, D.; Zhao, Y.; Dong, J.; Wang, J.; Shen, X. NPLC0393 from Gynostemma Pentaphyllum Ameliorates Alzheimer's Disease-like Pathology in Mice by Targeting Protein Phosphatase Magnesium-Dependent 1A Phosphatase. *Phytotherapy Research* **2023**, *37* (10), 4771–4790. https://doi.org/10.1002/ptr.7945.
(61) Ikegami, K.; Kimura, T.; Katsuragi, S.; Ono, T.; Yamamoto, H.; Miyamoto, E.; Miyakawa, T. Immunohistochemical Examination of Phosphorylated Tau in Granulovacuolar Degeneration Granules. *Psychiatry Clin Neurosci* **1996**, *50* (3), 137–140. https://doi.org/10.1111/j.1440-1819.1996.tb01678.x.
(62) Herrmann, M.; Golombowski, S.; Kräuchi, K.; Frey, P.; Mourton-Gilles, C.; Hulette, C.; Rosenberg, C.; Müller-Spahn, F.; Hock, C. ELISA-Quantitation of Phosphorylated Tau Protein in the Alzheimer's Disease Brain. *European Neurology* **1999**, *42* (4), 205–210. https://doi.org/10.1159/000008108.
(63) Hanes, J.; Kovac, A.; Kvartsberg, H.; Kontsekova, E.; Fialova, L.; Katina, S.; Kovacech, B.; Stevens, E.; Hort, J.; Vyhnalek, M.; Boonkamp, L.; Novak, M.; Zetterberg, H.; Hansson, O.; Scheltens, P.; Blennow, K.; Teunissen, C. E.; Zilka, N. Evaluation of a Novel Immunoassay to Detect P-Tau Thr217 in the CSF to Distinguish Alzheimer Disease from Other Dementias. *Neurology* **2020**, *95* (22), e3026–e3035. https://doi.org/10.1212/WNL.0000000000010814.
(64) Suárez-Calvet, M.; Karikari, T. K.; Ashton, N. J.; Lantero Rodríguez, J.; Milà-Alomà, M.; Gispert, J. D.; Salvadó, G.; Minguillon, C.; Fauria, K.; Shekari, M.; Grau-Rivera, O.; Arenaza-Urquijo, E. M.; Sala-Vila, A.; Sánchez-Benavides, G.; González-de-Echávarri, J. M.; Kollmorgen, G.; Stoops, E.; Vanmechelen, E.; Zetterberg, H.; Blennow, K.; Molinuevo, J. L.; for the ALFA Study; Beteta, A.; Cacciaglia, R.; Cañas, A.; Deulofeu, C.; Cumplido, I.; Dominguez, R.; Emilio, M.; Falcon, C.; Fuentes, S.; Hernandez, L.; Huesa, G.; Huguet, J.; Marne, P.; Menchón, T.; Operto, G.; Polo, A.; Pradas, S.; Soteras, A.; Vilanova, M.; Vilor-Tejedor, N. Novel Tau Biomarkers Phosphorylated at T181, T217 or T231 Rise in the Initial Stages of the Preclinical Alzheimer's Continuum When Only Subtle Changes in Aβ Pathology Are Detected. *EMBO Molecular Medicine* **2020**, *12* (12), e12921. https://doi.org/10.15252/emmm.202012921.
(65) Janelidze, S.; Stomrud, E.; Smith, R.; Palmqvist, S.; Mattsson, N.; Airey, D. C.; Proctor, N. K.; Chai, X.; Shcherbinin, S.; Sims, J. R.; Triana-Baltzer, G.; Theunis, C.; Slemmon, R.; Mercken, M.; Kolb, H.; Dage, J. L.; Hansson, O. Cerebrospinal Fluid P-Tau217 Performs Better than p-Tau181 as a Biomarker of Alzheimer's Disease. *Nat Commun* **2020**, *11* (1), 1683. https://doi.org/10.1038/s41467-020-15436-0.
(66) Ashton, N. J.; Pascoal, T. A.; Karikari, T. K.; Benedet, A. L.; Lantero-Rodriguez, J.; Brinkmalm, G.; Snellman, A.; Schöll, M.; Troakes, C.; Hye, A.; Gauthier, S.; Vanmechelen, E.; Zetterberg, H.; Rosa-Neto, P.; Blennow, K. Plasma P-Tau231: A New Biomarker for Incipient Alzheimer's Disease Pathology. *Acta Neuropathol* **2021**, *141* (5), 709–724. https://doi.org/10.1007/s00401-021-02275-6.
(67) Therriault, J.; Woo, M. S.; Salvadó, G.; Gobom, J.; Karikari, T. K.; Janelidze, S.; Servaes, S.; Rahmouni, N.; Tissot, C.; Ashton, N. J.; Benedet, A. L.; Montoliu-Gaya, L.; Macedo, A. C.; Lussier, F. Z.; Stevenson, J.; Vitali, P.; Friese, M. A.; Massarweh, G.; Soucy, J.-P.; Pascoal, T. A.; Stomrud, E.; Palmqvist, S.; Mattsson-Carlgren, N.; Gauthier, S.; Zetterberg, H.; Hansson, O.; Blennow, K.; Rosa-Neto, P. Comparison of Immunoassay- with Mass Spectrometry-Derived p-Tau Quantification for the Detection of Alzheimer's Disease Pathology. *Molecular Neurodegeneration* **2024**, *19* (1), 2. https://doi.org/10.1186/s13024-023-00689-2.
(68) Dammer, E. B.; Lee, A. K.; Duong, D. M.; Gearing, M.; Lah, J. J.; Levey, A. I.; Seyfried, N. T. Quantitative Phosphoproteomics of Alzheimer's Disease Reveals Cross-Talk between Kinases and Small Heat Shock Proteins. *Proteomics* **2015**, *15* (2–3), 508–519. https://doi.org/10.1002/pmic.201400189.

(69) Xia, Q.; Cheng, D.; Duong, D. M.; Gearing, M.; Lah, J. J.; Levey, A. I.; Peng, J. Phosphoproteomic Analysis of Human Brain by Calcium Phosphate Precipitation and Mass Spectrometry. *J Proteome Res* **2008**, *7* (7), 2845–2851. https://doi.org/10.1021/pr8000496.
(70) Fíla, J.; Honys, D. Enrichment Techniques Employed in Phosphoproteomics. *Amino Acids* **2012**, *43* (3), 1025–1047. https://doi.org/10.1007/s00726-011-1111-z.
(71) Dodds, J. N.; Baker, E. S. Ion Mobility Spectrometry: Fundamental Concepts, Instrumentation, Applications, and the Road Ahead. *J Am Soc Mass Spectrom* **2019**, *30* (11), 2185–2195. https://doi.org/10.1007/s13361-019-02288-2.
(72) Avila, J.; Lucas, J. J.; Pérez, M.; Hernández, F. Role of Tau Protein in Both Physiological and Pathological Conditions. *Physiological Reviews* **2004**, *84* (2), 361–384. https://doi.org/10.1152/physrev.00024.2003.
(73) Drewes, G.; Ebneth, A.; Preuss, U.; Mandelkow, E. M.; Mandelkow, E. MARK, a Novel Family of Protein Kinases That Phosphorylate Microtubule-Associated Proteins and Trigger Microtubule Disruption. *Cell* **1997**, *89* (2), 297–308. https://doi.org/10.1016/s0092-8674(00)80208-1.
(74) Huhe, H.; Shapley, S. M.; Duong, D.; Wu, F.; Ha, S.-K.; Choi, S.-H.; Kofler, J.; Mou, Y.; Guimaraes, T. R.; Thathiah, A.; Schaeffer, L. K. H.; Carter, G. W.; Seyfried, N. T.; Silva, A. C.; Sukoff Rizzo, S. J. Marmosets as Model Systems for the Study of Alzheimer's Disease and Related Dementias: Substantiation of Physiological Tau 3R and 4R Isoform Expression and Phosphorylation. *bioRxiv* **2024**, 2024.04.26.590453. https://doi.org/10.1101/2024.04.26.590453.
(75) Abreha, M. H.; Ojelade, S.; Dammer, E. B.; McEachin, Z. T.; Duong, D. M.; Gearing, M.; Bassell, G. J.; Lah, J. J.; Levey, A. I.; Shulman, J. M.; Seyfried, N. T. TBK1 Interacts with Tau and Enhances Neurodegeneration in Tauopathy. *J Biol Chem* **2021**, *296*, 100760. https://doi.org/10.1016/j.jbc.2021.100760.
(76) Shapley, S. M.; Shantaraman, A.; Kearney, M. A.; Dammer, E. B.; Duong, D. M.; Bowen, C. A.; Bagchi, P.; Guo, Q.; Rangaraju, S.; Seyfried, N. T. Proximity Labeling of the Tau Repeat Domain Enriches RNA-Binding Proteins That Are Altered in Alzheimer's Disease and Related Tauopathies. bioRxiv January 22, 2025, p 2025.01.22.633945. https://doi.org/10.1101/2025.01.22.633945.
(77) Yu, L.-R.; Veenstra, T. D. Characterization of Phosphorylated Proteins Using Mass Spectrometry. *Curr Protein Pept Sci* **2021**, *22* (2), 148–157. https://doi.org/10.2174/1389203721999201123200439.
(78) Gerritsen, J. S.; White, F. M. Phosphoproteomics: A Valuable Tool for Uncovering Molecular Signaling in Cancer Cells. *Expert Rev Proteomics* **2021**, *18* (8), 661–674. https://doi.org/10.1080/14789450.2021.1976152.
(79) Srinivasan, A.; Sing, J. C.; Gingras, A.-C.; Röst, H. L. Improving Phosphoproteomics Profiling Using Data-Independent Mass Spectrometry. *J. Proteome Res.* **2022**, *21* (8), 1789–1799. https://doi.org/10.1021/acs.jproteome.2c00172.
(80) Wang, Y.; Zhang, Y.; Hu, W.; Xie, S.; Gong, C.-X.; Iqbal, K.; Liu, F. Rapid Alteration of Protein Phosphorylation during Postmortem: Implication in the Study of Protein Phosphorylation. *Sci Rep* **2015**, *5* (1), 15709. https://doi.org/10.1038/srep15709.
(81) Takei, Y.; Teng, J.; Harada, A.; Hirokawa, N. Defects in Axonal Elongation and Neuronal Migration in Mice with Disrupted Tau and Map1b Genes. *J Cell Biol* **2000**, *150* (5), 989–1000.
(82) Ramkumar, A.; Jong, B. Y.; Ori-McKenney, K. M. ReMAPping the Microtubule Landscape: How Phosphorylation Dictates the Activities of Microtubule-Associated Proteins. *Developmental Dynamics* **2018**, *247* (1), 138–155. https://doi.org/10.1002/dvdy.24599.
(83) Kimura, T.; Yamamoto, H.; Takamatsu, J.; Yuzuriha, T.; Miyamoto, E.; Miyakawa, T. Phosphorylation of MARCKS in Alzheimer Disease Brains. *NeuroReport* **2000**, *11* (4), 869.
(84) Brudvig, J. J.; Weimer, J. M. X MARCKS the Spot: Myristoylated Alanine-Rich C Kinase Substrate in Neuronal Function and Disease. *Front. Cell. Neurosci.* **2015**, *9*. https://doi.org/10.3389/fncel.2015.00407.
(85) Leutert, M.; Rodríguez-Mias, R. A.; Fukuda, N. K.; Villén, J. R2-P2 Rapid-robotic Phosphoproteomics Enables Multidimensional Cell Signaling Studies. *Molecular Systems Biology* **2019**, *15* (12), e9021. https://doi.org/10.15252/msb.20199021.
(86) Bai, B.; Tan, H.; Peng, J. Quantitative Phosphoproteomic Analysis of Brain Tissues. In *Neuroproteomics*; Humana Press, New York, NY, 2017; pp 199–211. https://doi.org/10.1007/978-1-4939-6952-4_8.
(87) Schlosser, A.; Pipkorn, R.; Bossemeyer, D.; Lehmann, W. D. Analysis of Protein Phosphorylation by a Combination of Elastase Digestion and Neutral Loss Tandem Mass Spectrometry. *Anal Chem* **2001**, *73* (2), 170–176. https://doi.org/10.1021/ac000826j.
(88) Dickhut, C.; Feldmann, I.; Lambert, J.; Zahedi, R. P. Impact of Digestion Conditions on Phosphoproteomics. *J. Proteome Res.* **2014**, *13* (6), 2761–2770. https://doi.org/10.1021/pr401181y.
(89) A. Solari, F.; Dell'Aica, M.; Sickmann, A.; P. Zahedi, R. Why Phosphoproteomics Is Still a Challenge. *Molecular BioSystems* **2015**, *11* (6), 1487–1493. https://doi.org/10.1039/C5MB00024F.
(90) Goedert, M. Tau Protein and the Neurofibrillary Pathology of Alzheimer's Disease. *Trends in Neurosciences* **1993**, *16* (11), 460–465. https://doi.org/10.1016/0166-2236(93)90078-Z.
(91) Goedert, M.; Jakes, R.; Spillantini, M. G.; Hasegawa, M.; Smith, M. J.; Crowther, R. A. Assembly of Microtubule-Associated Protein Tau into Alzheimer-like Filaments Induced by Sulphated Glycosaminoglycans. *Nature* **1996**, *383* (6600), 550–553. https://doi.org/10.1038/383550a0.

(92) Spillantini, M. G.; Goedert, M. Tau Protein Pathology in Neurodegenerative Diseases. *Trends in Neurosciences* **1998**, *21* (10), 428–433. https://doi.org/10.1016/S0166-2236(98)01337-X.
(93) Samimi, N.; Sharma, G.; Kimura, T.; Matsubara, T.; Huo, A.; Chiba, K.; Saito, Y.; Murayama, S.; Akatsu, H.; Hashizume, Y.; Hasegawa, M.; Farjam, M.; Shahpasand, K.; Ando, K.; Hisanaga, S. Distinct Phosphorylation Profiles of Tau in Brains of Patients with Different Tauopathies. *Neurobiology of Aging* **2021**, *108*, 72–79. https://doi.org/10.1016/j.neurobiolaging.2021.08.011.
(94) Leutert, M.; Rodríguez-Mias, R. A.; Fukuda, N. K.; Villén, J. R2-P2 Rapid-Robotic Phosphoproteomics Enables Multidimensional Cell Signaling Studies. *Mol Syst Biol* **2019**, *15* (12), e9021. https://doi.org/10.15252/msb.20199021.